A Section 508–conformant HTML version of this article is available at https://doi.org/10.1289/EHP11580.

Multidimensional Analysis of Lung Lymph Nodes in a Mouse Model of Allergic Lung Inflammation following $PM_{2.5}$ and Indeno[1,2,3-*cd*]pyrene Exposure

Kwei-Yan Liu,[1,2,3] Yajing Gao,[2,3*] Wenfeng Xiao,[2,3*] Jinrong Fu,[2,4*] Saihua Huang,[2,3] Xiao Han,[2,3] Shih-Hsien Hsu,[5] Xiaojun Xiao,[6] Shau-Ku Huang,[1,6,7,8] and Yufeng Zhou[2,3]*

[1]Department of Respirology & Allergy, Third Affiliated Hospital of Shenzhen University, Shenzhen, China
[2]Institute of Pediatrics, Children's Hospital of Fudan University, National Children's Medical Center, and the Shanghai Key Laboratory of Medical Epigenetics, International Co-laboratory of Medical Epigenetics and Metabolism, Ministry of Science and Technology, Institutes of Biomedical Sciences, Fudan University, Shanghai, China
[3]National Health Commission (NHC) Key Laboratory of Neonatal Diseases, Fudan University, Shanghai, China
[4]Department of General Medicine, Children's Hospital of Fudan University, Shanghai, China
[5]Graduate Institute of Medicine, College of Medicine, Kaohsiung Medical University, Kaohsiung, Taiwan
[6]Institute of Allergy and Immunology, School of Medicine, Shenzhen University, Shenzhen, China
[7]National Institute of Environmental Health Sciences, National Health Research Institutes, Taiwan
[8]Department of Medicine, Johns Hopkins University School of Medicine, Baltimore, Maryland, USA

Background: Ambient particulate matter with an aerodynamic diameter of ≤2.5 μm ($PM_{2.5}$) is suggested to act as an adjuvant for allergen-mediated sensitization and recent evidence suggests the importance of T follicular helper (Tfh) cells in allergic diseases. However, the impact of $PM_{2.5}$ exposure and its absorbed polycyclic aromatic hydrocarbon (PAHs) on Tfh cells and humoral immunity remains unknown.

Objectives: We aimed to explore the impact of environmental $PM_{2.5}$ and indeno[1,2,3-*cd*]pyrene (IP), a prominent PAH, as a model, on Tfh cells and the subsequent pulmonary allergic responses.

Methods: $PM_{2.5}$- or IP-mediated remodeling of cellular composition in lung lymph nodes (LNs) was determined by mass cytometry in a house dust mite (HDM)-induced mouse allergic lung inflammation model. The differentiation and function of Tfh cells *in vitro* were analyzed by flow cytometry, quantitative reverse transcription polymerase chain reaction, enzyme-linked immunosorbent assay, chromatin immunoprecipitation, immunoprecipitation, and western blot analyses.

Results: Mice exposed to $PM_{2.5}$ during the HDM sensitization period demonstrated immune cell population shifts in lung LNs as compared with those sensitized with HDM alone, with a greater number of differentiated Tfh2 cells, enhanced allergen-induced immunoglobulin E (IgE) response and pulmonary inflammation. Similarly enhanced phenotypes were also found in mice exposed to IP and sensitized with HDM. Further, IP administration was found to induce interleukin-21 (*Il21*) and *Il4* expression and enhance Tfh2 cell differentiation *in vitro*, a finding which was abrogated in aryl hydrocarbon receptor (AhR)-deficient $CD4^+$ T cells. Moreover, we showed that IP exposure increased the interaction of AhR and cellular musculoaponeurotic fibrosarcoma (c-Maf) and its occupancy on the *Il21* and *Il4* promoters in differentiated Tfh2 cells.

Discussion: These findings suggest that the $PM_{2.5}$ (IP)–AhR–c-Maf axis in Tfh2 cells was important in allergen sensitization and lung inflammation, thus adding a new dimension in the understanding of Tfh2 cell differentiation and function and providing a basis for establishing the environment–disease causal relationship. https://doi.org/10.1289/EHP11580

Introduction

T helper 2 (Th2) cells have long been considered to mainly regulate the pathogenic manifestations of allergic asthma, such as immunoglobulin E (IgE)–mediated sensitization, airway hyperresponsiveness, and eosinophil infiltration.[1] However, more recent work has demonstrated that interleukin 4-positive ($IL\text{-}4^+$) T follicular helper (Tfh) cells, not Th2 cells, are required for IgE production.[2–5] Tfh cells are identified by their unique phenotype, which includes high expression levels of several markers, such as CXC-chemokine receptor 5 (CXCR5), inducible T-cell co-stimulator (ICOS), programmed cell death protein 1 (PD1), B-cell lymphoma 6 (Bcl-6, a transcriptional repressor), and IL-21 (a cytokine).[6] Tfh cells are the primary helper T-cell subset responsible for directing the affinity, longevity, and isotype of antibodies produced by B cells.[7,8] Owing to the fundamental role of Tfh cells in adaptive immunity, the stringent control of their production and function is critically important.

Tfh cell differentiation requires the cytokine milieu,[9] that is, IL-6 initiates Tfh cell development by activating the transcriptional factor signal transducer and activator of transcription 3 (Stat3) to induce transcriptional expression of *Bcl-6* and to repress type I interferon (IFN) signaling.[10,11] IL-21 is also critical for Tfh cell differentiation by inducing Bcl-6 and CXCR5 expression in an autocrine manner.[12,13] According to their cytokine and transcription factor profile, Tfh cells are classified into three subsets, namely, Tfh1, Tfh2, and Tfh13.[14] Tfh2 cells are distinguished from others by their ability to produce abundant quantities of IL-4.[15] A distinctive interleukin-4 (*Il4*) enhancer locus is bound by basic leucine zipper transcriptional factor activating transcription factor (ATF)–like (BATF) in Tfh2 cells, which is distinct from the regulatory element bound by GATA binding protein 3 (GATA3).[16] The Tfh2-derived IL-4 cytokine is critical for IgE induction, whereas IL-21 is critical for IgG1 induction.

It has been demonstrated that ambient particulate matter (PM) with an aerodynamic diameter of ≤2.5 μm ($PM_{2.5}$) acts as an adjuvant for IgE-mediated allergen sensitization in both animal and human studies.[17–19] However, the causal relationship and mechanisms have not been sufficiently established. Polycyclic aromatic hydrocarbons (PAHs) are a group of environmental pollutants mainly generated from the pyrolysis of organic matter and, in Asia, are mainly from traffic exhaust and industrial emissions.[20] These pollutants, which are abundantly adsorbed into $PM_{2.5}$,

*These authors contributed equally to this work.
Address correspondence to Yufeng Zhou, 399 Wanyuan Rd., Minhang, Shanghai 201102, China. Telephone: 86-21-64932907. Email: yfzhou1@fudan.edu.cn. And, Shau-Ku Huang, National Institute of Environmental Health Sciences, National Health Research Institutes, No. 35, Keyan Rd., Zhunan, 35053 Miaoli County, Taiwan. Email: skhuang@nhri.edu.tw
Supplemental Material is available online (https://doi.org/10.1289/EHP11580).
The authors declare that they have no relevant conflicts of interest.
Received 19 May 2022; Revised 23 January 2023; Accepted 9 February 2023; Published 28 March 2023.

generate reactive oxygen species and induce the oxidative stress associated with inflammation.[21] Recent studies have reported that PAHs are released from burning organic particles and interact with the intracellular aryl hydrocarbon receptor (AhR) to influence immune responses, highlighting the potential role of the $PM_{2.5}$–PAH–AhR axis in allergic diseases.[22,23] We previously reported that $PM_{2.5}$ and its associated PAHs disturb the balance of T helper 17 (Th17)/regulatory T (Treg) cells to aggravate allergic lung inflammation through AhR activation in a mouse model of asthma.[24] However, whether and how the $PM_{2.5}$–PAH–AhR axis affects antigen sensitization and humoral immune responses remain unclear. Based on a transcriptomics analysis of *in vitro* differentiated Tfh cells, increased expression of AhR has been reported during Tfh cell differentiation, suggesting the potential role of the AhR–PAH axis in regulating Tfh function and subsequent humoral immune responses, but the governing mechanisms are unknown.[25]

To this end, we employed a multidimensional approach, including single-cell mass cytometry, to explore the causal relationship between $PM_{2.5}$ exposure, remodeling of lymph node (LN) cells, humoral immunity, and allergen-induced pulmonary inflammation in a mouse model.

Materials and Methods

Mice

All mice used were on the C57BL/6 background. AhR-null mice (AhR KO; B6.129-*Ahr*^{tm1Bra}/J) and AhR^{loxp} [B6.129(FVB)-*Ahr*$^{tm3.1Bra}$/J] mice were purchased from the Jackson Laboratory. CD4-Cre mice [Tg (Cd4-cre)1Cwi/BfluJ] were obtained from Shanghai Model Organisms. AhR^{loxp} mice were crossed with *CD4*-Cre transgenic mice to obtain *Ahr*$^{fl/fl}$CD4-Cre mice (CD4$^{\Delta AhR}$) with *Ahr* deficiency in CD4$^+$ T cells. C57BL/6 mice were obtained from the SLAC Laboratory Animal Co. All animal experiments complied with the relevant laws and institutional guidelines as overseen by the Animal Studies Committee of the Children's Hospital of Fudan University (Shanghai, China). All the animals were housed, bred, and maintained under specific pathogen-free conditions with a temperature of $22 \pm 2^{\circ}C$ under a 12-h light/12-h dark cycle and 40%–70% relative humidity. All mice received sterile food and filtered water. A total of 101 mice at 6–8 wk of age were used in this study. A total of 11 mice [phosphate-buffered saline (PBS) group $n = 3$; house dust mite (HDM) group $n = 4$; HDM plus $PM_{2.5}$ group $n = 4$] were used for mass cytometry analysis. A total of 90 mice were used for the HDM-induced mouse allergic lung inflammation model in Figure 3 ($n = 10$ for each of the three groups, including PBS, HDM, and HDM plus IP) and Figure 4 ($n = 10$ for each of the six groups, including wild-type PBS [(WT_PBS), WT_HDM, WT_HDM plus $PM_{2.5}$, CD4$^{\Delta AhR}$_PBS, CD4$^{\Delta AhR}$_HDM, and CD4$^{\Delta AhR}$_HDM plus $PM_{2.5}$]. All mice were sacrificed in the automated carbon dioxide (CO_2) delivery system, and their lung-draining LNs and bronchoalveolar lavage fluids (BALFs) were individually harvested for subsequent flow cytometry analysis, and lung tissues were harvested and sectioned for hematoxylin and eosin (H&E) and periodic acid–Schiff (PAS) staining.

$PM_{2.5}$ and PAHs

$PM_{2.5}$ samples were continuously collected from June 2019 to December 2020 using Quartz fiber filters (1851-090; Whatman) and an air sampler (ZR-3930; Qingdao Junray Intelligent Instruments) on the open-air rooftop of the fourth floor of a research building of the Children's Hospital of Fudan University. Filter papers were replaced every 2 wk. The collected filter papers absorbing $PM_{2.5}$ were cut into small pieces, immersed in distilled water overnight at 4°C, and then sonicated (Skymon) for 30 min on three occasions. The $PM_{2.5}$ turbid liquid after sonication was filtered through sterile gauze, lyophilized to measure the weight, and stored at −20°C. The composition analysis of $PM_{2.5}$ (Figure S1A) was performed by China Certification & Inspection Group (CCIC) Physical and Chemical Testing Co., Ltd. In brief, ion chromatography was used for the detection of water-soluble cations and anions in $PM_{2.5}$ samples. Inductively coupled mass spectrometry (MS) was used for the determination of metal elements. A thermal–optical method was used for the determination of organic carbon and elemental carbon. For the composition analysis by CCIC, the PAHs in $PM_{2.5}$ (Figure S1B) were extracted, purified, and then analyzed by gas chromatography-MS (GC-MS; GC7890A-5975C; Agilent). $PM_{2.5}$ samples were extracted with 120 mL acetone/dichloromethane (1:1, vol/vol) in a Soxhlet extraction apparatus for 20 h to obtain PAHs data. After the completion of extraction, an internal standard (consisting of Acenaphthene-D10, Chrysene-D12, Naphthalene-D8, Phenanthrene-D10, and Pyrene-D12) was injected into the organic reagent to calibrate the concentration of each PAHs compound. Next, the filter was cut into pieces, and copper powder and anhydrous sodium sulfate were added to remove any contaminants. The extract was condensed with a rotary evaporator. Then, amorphous sodium sulfate, silica gel, and alumina were used to separate the aliphatic hydrocarbons and PAHs by the column. The elute solvent consisted of 15 mL hexane and 70 mL hexane/dichloromethane (3:7; vol/vol). The solvent was exchanged to hexane under vacuum afterward. The extracts were concentrated to 1 mL under a slow nitrogen stream in a 40°C water bath. The extracts were transferred into GC bottles with lids and stored at −20°C. The samples were analyzed by GC-MS (5975C; Agilent). One microliter of the sample was injected into a capillary column in splitless mode. The selected ion monitoring mode was used to collect the data. Helium was used as the carrier gas at a flow rate of 1.0 mL/min. The GC oven of the temperature program was 80°C for 1 min at the first stage, then it was increased to 235°C at a rate of 10°C/min. Next, it was increased to 300°C at a rate of 4°C/min and held for 4 min. The MS was operated in an electron impact model at 70 eV. For the animal experiment, the lyophilized $PM_{2.5}$ (6.25 μg/μL) was dissolved in PBS and stored at −20°C. Indeno[1,2,3-*cd*]pyrene (IP; ERI-001) was purchased from Sigma-Aldrich.

HDM-Induced Mouse Allergic Lung Inflammation Model

The HDM-induced mouse allergic lung inflammation model was established, as described previously,[26] with slight modifications. Briefly, 6- to 8-wk-old female C57BL/6 mice (Shanghai SLAC Experimental Animals) were exposed to light anesthesia (isoflurane). The mice were then suspended by their front incisors, and their tongues were gently extended to their lower mandibles. The different allergen solutions (HDM, HDM plus $PM_{2.5}$, or HDM plus IP) for different groups were delivered into the hypopharynx in 50-μL aliquots. The stock solutions were as follows: HDM (1 μg/μL; Cat# XPB91D3A2.5; Greer Laboratories) and $PM_{2.5}$ (6.25 μg/μL) were dissolved in PBS, and the stock solution of IP (10 mM) was dissolved in dimethyl sulfoxide (DMSO) and further diluted with PBS for the working concentration (6.25 μM). Mice in the HDM group were sensitized by intratracheal instillation of 10 μg of HDM dissolved in 50 μL of PBS per mouse on days 0, 1, and 2 and challenged on days 9, 10, 11, and 12 with the same amount of HDM. Mice in the HDM plus $PM_{2.5}$ group or the IP group were sensitized by intratracheal instillation of 10 μg of HDM mixed with $PM_{2.5}$ (250 μg/mouse) or IP (5 μM/mouse) in a final volume of 50 μL per mouse on days 0, 1, and 2 and challenged on days 9, 10, 11, and 12 with 10 μg of HDM only. Mice in the control group received 50 μL of PBS during the sensitization and the challenge phases. In addition, 0.05% equal concentrations of DMSO were used as the vehicle

control in PBS and HDM group to make the comparison with of HDM plus IP group.

Mass Cytometry and Data Analysis

Mass cytometry and data analysis were performed by Zhejiang Puluoting Health Tech Co., Ltd. Briefly, mice were sacrificed in an automated CO_2 delivery system on day 14, then the lung LNs of each mouse were harvested (PBS group $n=3$; HDM group $n=4$; HDM plus $PM_{2.5}$ group $n=4$). LNs were ground with a sterile syringe piston in Dulbecco's Modified Eagle Medium (DMEM) containing 10% fetal bovine serum (FBS), and filtered through a 70-μm cell strainer (Cat# 352350; BD Biosciences) to obtain a single-cell suspension. Then the cells were washed with PBS containing 0.5% bovine serum albumin (BSA) and centrifuged at $400\times g$ for 5 min at 4°C. Subsequently, 3×10^6 cells per sample were resuspended in 100 μL of Cell-ID Cisplatin-194Pt (250 nM; Cat# 201194; Fluidigm) solution for 5 min on ice, then the cells were washed twice by adding 1 mL of fluorescence-activated cell sorting (FACS) buffer (1 × PBS containing 2% FBS) and centrifuged at $400\times g$ for 5 min at 4°C. Then, to block Fc receptors, the cells were incubated with an antimouse CD16/32 monoclonal antibody (mAb) (clone 93; Cat# 101301; 1.0 μg mAb/10^6 cells; Biolegend) in a 100-μL volume for 10 min on ice before staining with a cocktail of metal-labeled mAbs against cell surface molecules. Cells were then treated with Fixation/Permeabilization Buffer (eBioscience) and further stained with an intracellular antibody cocktail. The cells were then incubated with Cell-ID Intercalator (191/193Ir; Cat# 201192A; Fluidigm) to discriminate single nucleated cells from doublets. The antibodies conjugated with isotopically pure elements are listed in Table S1. Then cells were washed twice with 2 mL of deionized water and centrifuged at $800\times g$ for 5 min at 4°C. Finally, the cells were resuspended with deionized water, added to 20% EQ beads (Cat# 201078; Fluidigm), and injected into the mass cytometer (Helios; Fluidigm). All instruments were evaluated to ensure performance at or above the minimum Helios system specifications for calibration. Following the instrument tuning and beads sensitivity test, the system was preconditioned with deionized water. A minimum of 300,000 events for lung LNs were acquired per file at a typical acquisition rate of 300 events/s. Prior to data analysis, the data of each sample were debarcoded from raw data using a doublet-filtering scheme with unique mass-tagged barcodes. All data files were normalized and manually gated by FlowJo software (version 10.8.1, BD Biosciences) to exclude debris, dead cells, and doublets, resulting in live, single $CD45^+$ immune cells. X-shift was applied to automatically identify distinct immune cell subsets. Dimensionality reduction algorithm t-stochastic neighbor embedding (t-SNE) was performed to visualize the high-dimensional data in two dimensions, showing the distribution of each cluster and marker expression, as well as the difference among each group or different samples. Heatmaps were generated according to the median value for the assigned markers in clusters.

Lung Pathology

The mouse lung tissues were collected individually from each of the experimental groups, as noted above, then perfused and fixed in 4% neutral-buffered formalin. Paraffin-embedded lung sections (5 μm) were stained with H&E or PAS according to the manufacturer's protocols (Wuhan Servicebio Technology). The severity of peribronchial inflammation was scored with H&E staining as follows: 0, normal; 1, few cells; 2, a ring of inflammatory cells 1-cell layer deep; 3, a ring of inflammatory cells 2- to 4-cells deep; and 4, a ring of inflammatory cells 4-cells deep. The severity of peribronchial inflammation was scored with PAS staining as follows: 0, PAS-positive cells ≤5%; 1, 5% < PAS-positive cells ≤25%; 2, 25% < PAS-positive cells ≤50%; 3, 50% < PAS-positive cells ≤75%; and 4, PAS-positive cells >75%.[24] For each mouse, three light fields were randomly selected and counted from one slide, and the mean score was calculated.

T Cell Isolation and Differentiation in Vitro

Splenic CD4-naïve T cells were isolated from 6-wk-old female C57BL/6 mice using a Naïve $CD4^+$ T Cell Isolation kit (Cat# 130-104-453; Miltenyi Biotec). Approximately 2×10^5 cells in 200 μL were seeded into 96-well plates precoated with 1 μg/mL of anti-CD28 (37.51; Cat# 553295; BD Biosciences) and 1 μg/mL of anti-CD3e (145-2C11; Cat# 553058; BD Biosciences). For cells cultured under Tfh cell–skewing conditions with some modifications, as described previously,[27] the medium was supplemented with anti-interferon-gamma (anti-IFN-γ; XMG1.2; 15 μg/mL; Cat# BE0055; Bioxcell), anti-IL-4 (11B11; 15 μg/mL; Cat# BE0045; Bioxcell), anti-IL-2 (JES6-5H4; 15 μg/mL; Cat#BE0042; Bioxcell), and IL-6 (15 ng/mL; Cat#216-16; Peprotech). Immature T helper (Th0) cells were cultured under the same conditions without IL-6. IP at the specified concentration (30 nM or 300 nM) and an AhR inhibitor (CH223191, 10 μM) was added to the medium 6 h after initial cell plating. IP and CH223191 were dissolved in DMSO. The stock solution was further diluted with PBS for the working solution. A 0.01% equal concentration of DMSO was used in the control group as the vehicle control. Cells were cultured for 6 d before analysis.

Lentivirus Packaging and Infection

pLKO.1-c-Maf short hairpin RNA (shRNA; lentivirus plasmid; Cat# TRCN0000208001; RNAi Core Facility), pCMV-ΔR8.91 (packaging plasmid; Cat# C6-6-1; RNAi Core Facility), and pMD.G (envelope plasmid; Cat# C6-6-1; RNAi Core Facility) were transfected into 293T cells (ATCC) using TransIT-LT1 (Cat# MIR2300; Mirus Bio). The lentiviral supernatant was harvested 48 h after transfection. Splenic CD4-naïve T cells were isolated from three 6-wk-old female C57BL/6 mice using a Naïve $CD4^+$ T Cell Isolation kit. Naïve $CD4^+$ T cells were stimulated with the plate-bound anti-CD3e (5 μg/mL) and anti-CD28 (5 μg/mL) under neutral conditions (10 μg/mL anti-IFN-γ and 10 μg/mL anti-IL4) for 20 h. Lentiviral supernatant was added to the cell culture medium in the presence of polybrene (4 μg/mL) with centrifugation (1,800 rpm at 32°C) for 90 min, and the medium was exchanged with fresh medium 4 h after infection. One day after infection, the cells were cultured under Tfh cell–skewing conditions for 6 d before analysis.

Quantitative Reverse Transcription Polymerase Chain Reaction

Total RNA was extracted from cells using TRIzol Reagent (Invitrogen), and the concentration and quality (OD260/280 between 1.9 and 2.1 is qualified) of RNA were determined by NanoDrop (Thermo Fisher). Single-stranded complementary DNA (cDNA) was synthesized using the PrimeScript II first Strand cDNA Synthesis Kit (Takara). Quantitative reverse transcription polymerase chain reaction (RT-qPCR) was performed with SYBR Premix Ex Taq II (Takara) using the Roche 480 Real Time PCR System (denature: 1 cycle for 95°C, 30 s; PCR: 40 cycles for 95°C, 5 s and 60°C, 30 s; cooling: 1 cycle for 50°C, 30 s). The mRNA expression levels of target genes were normalized to β-actin using the $2^{-\Delta\Delta Ct}$ method. The PCR primers used are provided in Table S2.

Antibodies and Flow Cytometry

BALF was harvested by two consecutive flushes of the lung with 0.8 mL of ice-cold PBS. The total cell numbers were counted

with default count settings using a Countess II Automated Cell Counter (Thermo Fisher). Differential cell counts in BALF were obtained by flow cytometry, as previously described. BALF cells were stained with the following antibodies (all of which were from eBioscience): PE anti-Siglec-F (1RNM44N; Cat# 12-1702-80; 0.2 μg mAb/1×10^6 cells), fluorescein isothiocyanate anti-alpha-mac3 (M1/70; Cat# 85-11-0112-82; 0.2 μg mAb/1×10^6 cells), allophycocyanin (APC) anti-Gr-1 (RB6-8C5; Cat# 85-94-5931-71; 0.2 μg mAb/1×10^6 cells), Percp-Cy5.5 anti-CD3e (145-2C11; Cat# 85-15-0031-63, 0.1 μg mAb/1×10^6 cells), and Percp-Cy5.5 anti-CD19 (MB19-1; Cat# 85-15-0191-81; 0.1 μg mAb/1×10^6 cells). The cells were then washed twice by adding 1 mL of FACS buffer (PBS containing 2% FBS) and centrifuged at $400 \times g$ for 5 min at 4°C. Finally, the cells were resuspended with 300 μL of FACS buffer, and 1×10^4 cells per sample were collected and analyzed on a BD FACS Canto II flow cytometer (BD Biosciences). Data were analyzed by FlowJo software (version 10.8.1, BD Biosciences). Eosinophils were determined as side scatter $(SSC)^{high}SiglecF^{+}Mac\text{-}3^{-}$ cells, and alveolar macrophages cells were gated as $SSC^{high}SiglecF^{+}Mac\text{-}3^{+}$ cells. Granulocytes were gated as SSC^{high} $Gr\text{-}1^{+}$ cells, and lymphocytes were gated as forward scatter $(FSC)^{low}/SSC^{low}$ $CD3e^{+}$ or $CD19^{+}$. For analysis of Tfh cells in lung LNs, the LNs were harvested, ground with a sterile syringe piston in DMEM containing 10% FBS, and filtered through a 70-μm cell strainer (Cat# 352350; BD Biosciences) to obtain a single-cell suspension. Then the cells were washed with PBS containing 2% FBS and centrifuged at $400 \times g$ for 5 min at 4°C. Subsequently, 5×10^6 cells per sample were resuspended in 100 μL of an antibody cocktail comprising anti-CD4-FITC (H129.19; Cat# 100540; 0.01 μg mAb/1×10^6 cells; Biolegend), anti-CD19-Percp-cy5.5 (1D3/CD19; Cat# 115530; 0.01 μg mAb/1×10^6 cells; Biolegend), anti-ICOS-PE (15F9; Cat# 107706; 0.02 μg mAb/1×10^6 cells; Biolegend), anti-CXCR5-biotin (2G8; Cat# 551960; 0.1 μg mAb/1×10^6 cells; BD Biosciences), and anti-PD1-PE-cy7 (RMP1-30; Cat# 109110; 0.02 μg mAb/1×10^6 cells; Biolegend) at 4°C for 30 min in the dark. The cells were then washed and stained with streptavidin-BV421 (Cat# 405225; 0.1 μg mAb/1×10^6 cells; Biolegend) in 100 μL of solution at 4°C for 30 min in the dark. For transcription factor staining, the cells were washed and fixed with the Foxp3 Fixation/Permeabilization buffer set (Cat# 20201221; eBioscience) at 4°C overnight, according to the manufacturer's instructions. One day later, the cells were washed, resuspended, and stained with anti-Foxp3-APC (FJK-16s; Cat# 20201221; 0.04 μg mAb/1×10^6 cells; eBioscience) in 100 μL of solution at room temperature for 30 min. The cells were washed with 1 mL $1 \times$ Perm/Wash buffer and centrifuged at $600 \times g$ for 5 min at 4°C for the first time and again washed with 1 mL of FACS buffer (PBS containing 2% FBS), centrifuged at $600 \times g$ for 5 min at 4°C. Then the cells were resuspended in 300 μL of FACS buffer. Finally, 1×10^5 cells per sample were collected and analyzed on a BD FACS Canto II flow cytometer (BD Biosciences). For analysis of *in vitro* Tfh cell differentiation, the cells were first stained with the surface markers mentioned above, followed by intracellular staining with antimouse Bcl-6-PerCP-eflour 710 (BCL-DWM; Cat# 46-5453-82; 0.02 μg mAb/1×10^6 cells; eBioscience) or PerCP-eflour 710-conjugated rat IgG2a isotype control (eBR2a; Cat# 46-4321-80; 0.02 μg mAb/1×10^6 cells; eBioscience) using the Foxp3 Fixation/Permeabilization buffer set (Cat# 20201221; eBioscience). Finally, $>1 \times 10^4$ cells per sample were collected and analyzed on a BD FACS Canto II flow cytometer (BD Biosciences). Data were analyzed by FlowJo software (version 10.8.1, BD Biosciences).

Enzyme-Linked Immunosorbent Assay

Levels of total serum IgE and IgG1 were measured by a mouse IgE uncoated enzyme-linked immunosorbent assay (ELISA) kit (Cat# 88-50460-22; Invitrogen) and IgG1 uncoated ELISA kit (Cat# 88-50410-22; Invitrogen) according to the manufacturer's instructions. Briefly, 96-well plates were coated with antimouse IgE or IgG1. After blocking, the diluted serum samples were added into the wells and incubated for 2 h at room temperature. After incubation, the plates were washed with phosphate buffered solution with 0.1% tween-20 (PBST), and the antimouse IgE- or IgG1-conjugated biotin was added and incubated for 1 h at room temperature. The plate was then washed and incubated with streptavidin–horseradish peroxidase (HRP) for 30 min at room temperature in the dark. Finally, tetramethylbenzidine substrate was added, and the reaction was stopped by sulfuric acid. The absorbance at 450 nm was measured using a plate reader. For the HDM-specific IgG1 ELISA, plates were coated with HDM (50 μg/mL) followed by secondary reagents, as mentioned above. For the measurement of HDM-specific IgE levels, serum IgG was first depleted with Protein G magnetic beads (Beyotime).[28] Similarly, plates were coated with HDM (50 μg/mL), and, after blocking, the serum sample with IgG depletion was added and incubated at 4°C overnight. Biotin-conjugated antimouse IgE was added followed by the addition of streptavidin-HRP and tetramethylbenzidine substrate. Finally, the absorbance was read at 450 nm using a plate reader.

Chromatin Immunoprecipitation

The chromatin immunoprecipitation (ChIP) assay was performed using the Pierce Magnetic ChIP Kit (Cat# 26157; Thermo Fisher) according to the manufacturer's instructions. Briefly, cells were fixed with 1% formaldehyde for 10 min and quenched with 0.125 M glycine for 5 min. The chromatin was fragmented by micrococcal nuclease digestion. The chromatin was immunoprecipitated with an anti-AhR antibody (dilution 1:50; Cat# SA-210; Biomol) or anti-Maf antibody (dilution 1:50; Cat# GTX129420; GeneTex) overnight at 4°C. The antibody–chromatin complexes were then pulled down by ChIP-Grade Protein A/G Magnetic Beads and eluted with the elution buffer provided in the ChIP Kit. After incubation at 65°C for cross-link reversal, the samples were digested by RNase A and proteinase K. The immunoprecipitated DNA was collected using a DNA Clean-Up Column. DNA was quantified by qPCR using SYBR Premix Ex Taq II (Takara). The PCR primers used are provided in Table S3.

Immunoprecipitation and Western Blotting

Cell lysis was performed using Pierce IP Lysis Buffer (Cat# 87787; Thermo Fisher), and the sample was then subjected to ultrasonic treatment (Cat# JP-010T; Skymen), followed by centrifugation at $16{,}000 \times g$ for 15 min at 4°C. The protein concentration of harvested supernatants was quantified by the Bicinchoninic Acid (BCA) Assay Kit (Cat# T9300A; Takara), and 500 μg of protein in a 500-μL volume was incubated overnight at 4°C with anti-AhR antibody (5 μg; Cat# SA-210; Biomol) or IgG antibody (1U6H0; 5 μg; Cat# MA5-42729; Thermo Fisher) with gentle rotation. Protein A/G Magnetic Beads (Cat# 88802-3; Thermo Fisher) were first washed twice with PBS and then incubated with the previously described protein–antibody complexes for 2 h at 4°C with gentle rotation. Then the protein A/G magnetic beads were collected and washed three times with ice-cold PBS containing protease phosphatase inhibitor (Cat# 78440; Thermo Fisher) by magnetic frame. After being washed, the immunocomplexes were boiled with 60 -μL of 2× Laemmli sample buffer (Cat# 1610747; Bio-Rad) in 95°C for 5 min, and a 25-μL sample was loaded into a 12% sodium dodecyl sulfate–polyacrylamide gel electrophoresis gel and subjected to electrophoresis at 100 V for ∼90 min. Next, the proteins separated in the gel were transferred to polyvinylidene fluoride membranes (Cat# 88520; Thermo Fisher) at 0.18 A for 1.5 h. The membranes were then blocked in 5% BSA (Cat# ST023;

Beyotime) for 1 h, followed by incubation with primary antibodies overnight at 4°C. After being washed with 0.1% Tween-20–containing tris buffered saline solutions (TBST) three times, the membranes were incubated with HRP-conjugated goat-antirabbit or goat-antimouse antibody (1:5,000; Cell Signaling Technology) for 1 h. After being washed again with TBST three times, the bands were finally imaged using the chemiluminescent HRP substrate (Thermo Fisher) and a Molecular Imager ChemiDoc XRS+ Imaging System (Bio-Rad). The primary antibodies used were as follows: anti-c-Maf antibody (1:1,000; Cat# GTX129420; GeneTex), anti-AhR antibody (1:1,000), and anti-β-actin antibody (AC-15; 1:5,000; Cat# A5441; Sigma-Aldrich).

Statistical Analyses

All statistical analyses were performed using GraphPad Prism software (version 9.0). Unless otherwise stated, all statistical analyses were carried out through unpaired *t*-tests or one-way analysis of variance (ANOVA) followed by post hoc Bonferroni's multiple comparisons test multiple comparison tests, as appropriate. Data were considered statistically significant when $p < 0.05$ and presented as means ± standard errors of the mean (SEMs).

Results

Analysis of the Immune Cell Populations in Lung LNs and Measure of Allergen-Specific Antibody Production and Lung Inflammation in Mice Exposure to $PM_{2.5}$

To investigate the impact of $PM_{2.5}$ exposure on a well-established mouse model of airway inflammation, female C57BL/6 mice were intratracheally sensitized with saline control PBS, HDM, or HDM plus $PM_{2.5}$ daily from day 0 to day 2. The PBS group was challenged intratracheally with PBS; the HDM group and the HDM plus $PM_{2.5}$ group were challenged intratracheally with HDM from day 9 to day 12 (Figure 1A). Compared with the PBS and HDM groups, mice in the HDM plus $PM_{2.5}$ group showed significantly aggravated HDM-induced pulmonary inflammatory response, as evidenced by the recruitment of inflammatory cells in the lungs, dense peribronchial infiltrates, and goblet cell hyperplasia (Figure S2A–E), as well as by higher serum levels of total IgE, total IgG1, HDM-specific IgE, and HDM-specific IgG1 antibodies (Figure S2F–I).

To examine whether $PM_{2.5}$ exposure affects lung LN cell composition, LN cells were used for single-cell mass cytometry analysis with a panel of antibodies targeting lineage markers and cytokines associated with adaptive and innate immune systems. For the unsupervised detection of cell subsets, we applied the X-shift clustering algorithm, which divides the cells into phenotypically distinct clusters based on optimal *k*-nearest neighbor (*k*-NN) values. We also examined surface marker staining intensity on t-SNE dimension–reduced space, which visualizes the high-dimensional data. The t-SNE plot generated from the merged data represents a map of $CD45^+$ cells present in lung LNs. Based on lineage markers, we assessed the locations within the t-SNE plot of the following five major subsets: $CD4^+$ T cells, $CD8^+$ T cells, $CD4^-CD8^-$ T cells, $CD19^+$ B cells, and myeloid cells (Figure 1B).

As expected, exposure to HDM resulted in higher numbers of B cells compared with the control mice (PBS group). The HDM plus $PM_{2.5}$ group showed an even greater proportion and number of B cells compared with the PBS and HDM groups (Figure 1B–E). In addition, the t-SNE results showed that the expression of IgE in the HDM plus $PM_{2.5}$ group was significantly higher than that in the HDM or PBS group (Figure 1F). The percentages of IgE^+ B cells ($CD19^+IgE^+CD138^-$) and active IgE^+ B cells ($CD19^+IgE^+IgM^+IgD^+CD138^-$) were also higher following $PM_{2.5}$ exposure (Figures 1G,H and S3).

Because dendritic cells (DCs) are critical in initiating an immune response, we manually gated $CD11c^+$ myeloid cells (Figure S4A). Based on the t-SNE plot and marker density, we defined the following six clusters: migratory DC-1 ($MHCII^{hi}CD11c^{hi}PD\text{-}L1^+PD\text{-}L2^+CD11b^+CCR7^{hi}$), migratory DC-2 ($MHCII^{hi}CD11c^{int}PD\text{-}L1^{int}PD\text{-}L2^{int}CD11b^+CCR7^{hi}$), plasmacytoid DCs (pDCs; $MHCII^{lo}CD11c^{int}B220^+CD11b^-$), conventional DC1 (cDC1s; $MHCII^{hi}CD11c^{hi}B220^-CD8a^+CD11b^{lo}CCR7^-$), conventional DC2 (cDC2s; $MHCII^{int}CD11c^{hi}B220^-CD4^+CD8a^-CD11b^+CCR7^-$), and macrophages ($CD11c^{int}CD11b^{hi}F4/80^{hi}$; Figure S4B and Excel Table S14). An additional two clusters were identified as expressing low levels of major histocompatibility complex II (MHCII) or CD11c (Figure S4B).

Overall, the frequency of the migratory DC-1 subset was significantly higher in both the HDM and HDM plus $PM_{2.5}$ groups compared with the PBS group, whereas the migratory DC-2 subset was lower (Figure S4C–E). Further, our results showed that the frequency of cDC2s was significantly higher in the HDM and HDM plus $PM_{2.5}$ groups compared with the PBS group, whereas no significant differences were observed between the HDM and HDM plus $PM_{2.5}$ groups (Figure S4C,F). The frequency of the $CD11c^{low}$ subset was decreased in the HDM plus $PM_{2.5}$ group compared with the PBS group (Figure S4C,G). In addition, the frequencies of the $MHCII^{low}$, pDC, and cDC1 subsets were similar among the groups (Figure S4C,H–J). Interestingly, we noted that a relatively minor cell population, defined as macrophages ($CD11c^{int}CD11b^{hi}F4/80^{hi}$), was significantly higher in the HDM plus $PM_{2.5}$ group compared with the PBS and HDM groups (Figure S4C,K).

We next gated $CD45^+TCR\beta^+CD4^-CD8^+$ cells as $CD8^+$ T cells and divided $CD8^+$ T cells into the following four subsets by t-SNE analysis: naïve $CD8^+$ T cells ($CD44^-CD62L^+$), central memory $CD8^+$ T cells (Tcm, $CD44^+CD62L^+$), effector $CD8^+$ T-cell/effector memory $CD8^+$ T cells (Tem, $CD44^+CD62L^-$), and preeffector-like $CD8^+$ T cells ($CD44^-CD62L^-$; Figure S5A, B and Excel Table S23). The HDM and HDM plus $PM_{2.5}$ groups showed a significant decrease in the proportion of naïve $CD8^+$ T cells, but an increase in preeffector-like $CD8^+$ T cells and $CD8^+$ Tem cells compared with the PBS group, and no difference was found between the HDM plus $PM_{2.5}$ group and the HDM group during the sensitization phase. In addition, there was no difference in $CD8^+$ Tcm cells among the PBS, HDM, and HDM plus $PM_{2.5}$ groups (Figure S5C,D).

Mass Cytometry Analysis of the $CD4^+$ T-Cell Population in Lung LNs

Because $CD4^+$ T-cell subsets play crucial roles in the regulation of humoral immunity, we sorted the $CD4^+$ T cells and eliminated unrelated cell lineage markers for the unsupervised detection of $CD4^+$ T-cell subsets. We evaluated the locations within the t-SNE plot of the following five different subsets: naïve $CD4^+$ T cells ($TCR\beta^+CD4^+CD62L^+$), effector $CD4^+$ T cells ($TCR\beta^+CD4^+CD62L^-$), Treg cells ($TCR\beta^+CD4^+CD25^+Foxp3^+$), T follicular regulatory (Tfr) cells ($TCR\beta^+CD4^+CXCR5^+Foxp3^+$), and Tfh cells ($TCR\beta^+CD4^+CXCR5^+Bcl\text{-}6^+$) (Figure 2A,B and Excel Table S25). To further investigate whether $PM_{2.5}$ preferentially altered a specific $CD4^+$ T-cell subset, we determined the proportion and number of each subset among the PBS, HDM, and HDM plus $PM_{2.5}$ groups (Figure 2A). Naïve $CD4^+$ T cells were present at lower cell numbers and proportions in the HDM and HDM plus $PM_{2.5}$ groups compared with the PBS group (Figure 2C,D). Although the numbers and proportions of effector $CD4^+$ T cells, Treg cells, and Tfr cells were different between the

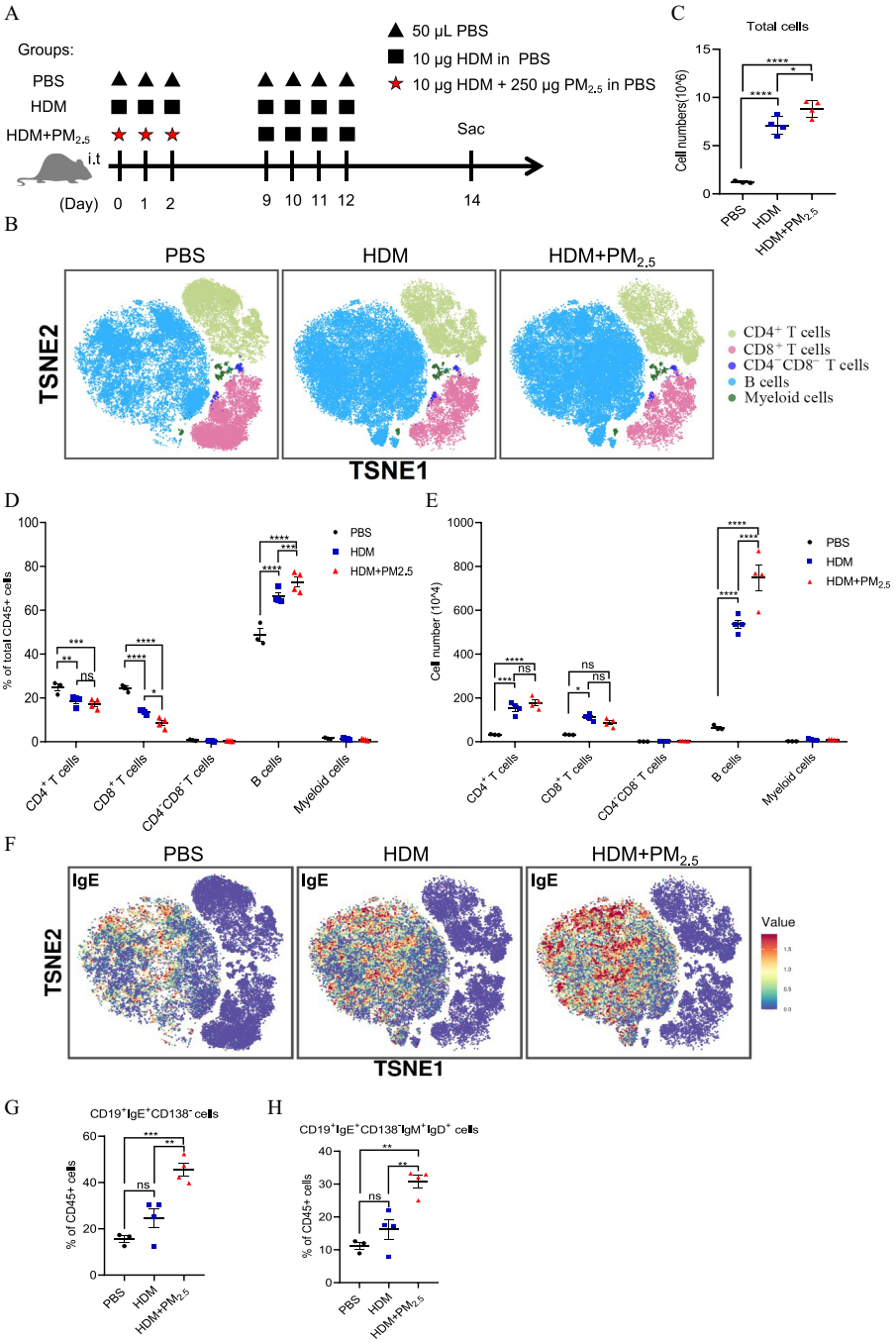

Figure 1. Mass cytometry analysis of the immune cell composition in lung LNs. (A) Schematic representation of the house dust mite (HDM)-induced mouse allergic lung inflammation model. Mice in the HDM group were sensitized by intratracheal inhalation of 10 μg of HDM dissolved in 50 μL of PBS per mouse on days 0, 1, and 2 and challenged on days 9, 10, 11, and 12 with the same amount of HDM. Mice in the HDM plus $PM_{2.5}$ group were sensitized by intratracheal inhalation of 10 μg of HDM mixed with $PM_{2.5}$ (250 μg/mouse) in a final volume of 50 μL per mouse on days 0, 1, and 2 and challenged on days 9, 10, 11, and 12 with 10 μg of HDM only. The PBS group mice received 50 μL of PBS during the sensitization and the challenge phases. (B) $CD45^+$ leukocytes in lung LNs were analyzed by mass cytometry (CyTOF; $n = 3$–4 samples per group) using a panel of 41 antibodies on day 14 (D14). t-SNE plot of $CD45^+$ compartments overlaid with color-coded clusters. An equal number of $CD45^+$ compartments in the lung LNs from the PBS, HDM, and HDM plus $PM_{2.5}$ groups was compared in the t-SNE plots. (C) Total cell number of lung LNs from each group (numerical values are shown in Excel Table S9). (D) Relative frequencies (numerical values are shown in Excel Table S10) and (E) cell numbers (numerical values are shown in Excel Table S11) of the indicated immune cell subsets among each group. (F) t-SNE plot of $CD45^+$ leukocytes overlaid with the expression of IgE among the PBS, HDM, and HDM plus $PM_{2.5}$ groups. The colors are coded according to the relative expression of the indicated IgE markers. Red indicates high expression, and blue indicates low expression. The percentages of (G) IgE-positive B cells ($CD19^+IgE^+CD138^-$) (numerical values are shown in Excel Table S12) and (H) activated IgE-positive B cells ($CD19^+IgE^+IgM^+IgD^+CD138^-$) (numerical values are shown in Excel Table S13) were manually gated by FlowJo software (version 10.8.1, BD Biosciences). Data are shown as the means ± SEMs. ns, not significant; $^*p < 0.05$, $^{**}p < 0.01$, $^{***}p < 0.001$, and $^{****}p < 0.0001$ according to ANOVA followed by Bonferroni's multiple comparisons test. Note: ANOVA, analysis of variance; Ig, immunoglobulin; i.t., intratracheally; LN, lymph node; PBS, phosphate-buffered saline; $PM_{2.5}$, ambient particulate matter with an aerodynamic diameter of ≤2.5 μm; SEM, standard error of the mean; t-SNE, t-stochastic neighbor embedding.

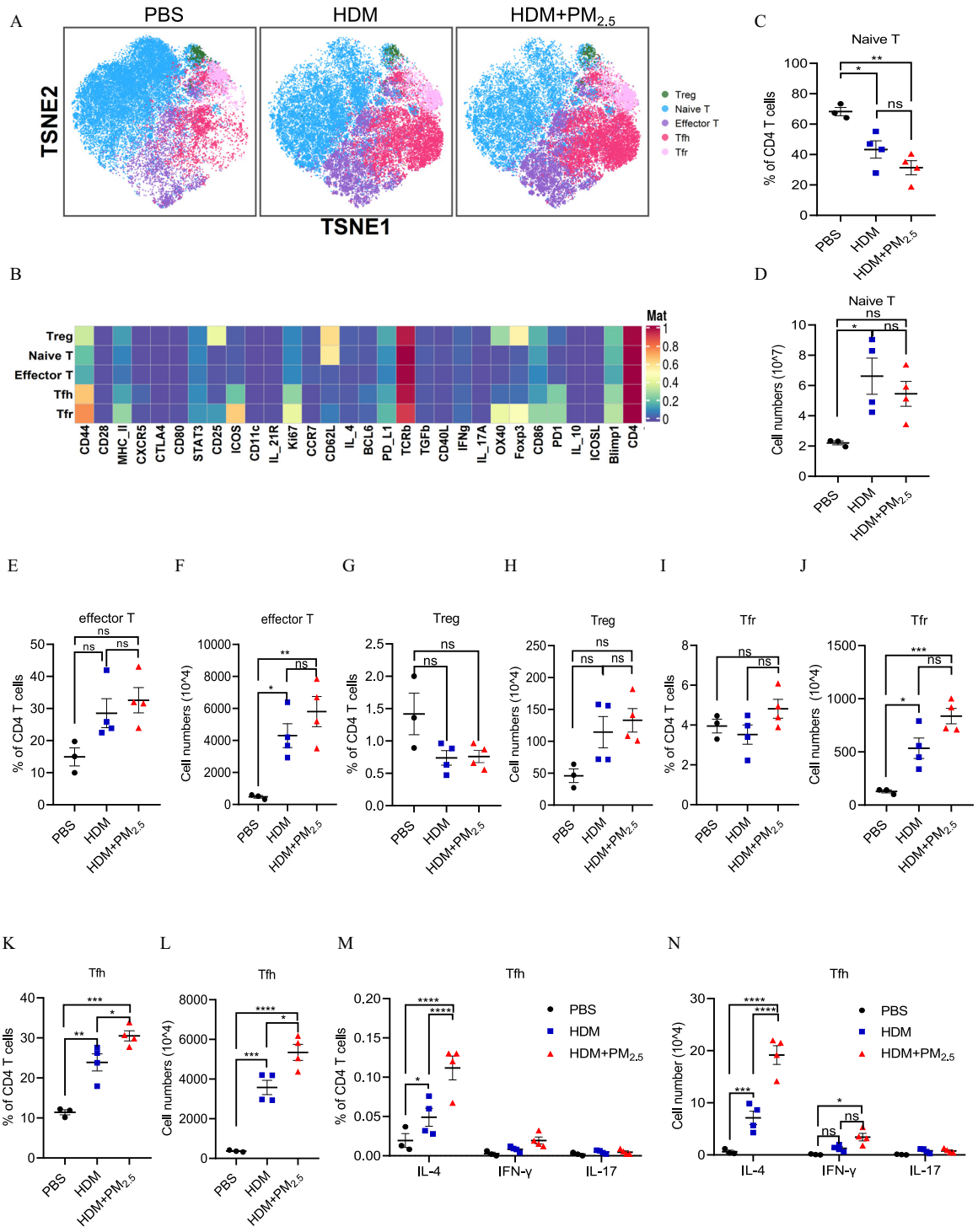

Figure 2. Mass cytometry analysis of the $CD4^+$ population shift in lung LNs. (A) The $CD4^+$ population, which was plotted by t-SNE, was separated into five clusters according to the expression of the indicated markers. t-SNE plots of an equal number of $CD4^+$ T cells from each treatment group. Each color represents the indicated $CD4^+$ T-cell subset. (B) Heatmap displaying normalized marker expression of each $CD4^+$ T-cell cluster (numerical values are shown in Excel Table S25). (C–L) Relative frequencies and numbers of $CD4^+$ T-cell subsets among the PBS, HDM, and HDM plus $PM_{2.5}$ groups (numerical values are shown in Excel Tables S26–S35). (M) Percentages of IL-4^+, IFN-γ^+, and IL-17^+ Tfh cells relative to $CD4^+$ T cells in each treatment group (numerical values are shown in Excel Table S36). (N) Numbers of IL-4^+, IFN-γ^+, and IL-17^+ Tfh cells in each treatment group (numerical values are shown in Excel Table S37). $n = 3$–4 per group. Data are shown as the means ± SEMs. ns, not significant; $^*p < 0.05$, $^{**}p < 0.01$, $^{***}p < 0.001$, and $^{****}p < 0.0001$ according to ANOVA followed by Bonferroni's multiple comparisons test. Note: ANOVA, analysis of variance; HDM, house dust mite; IFN, interferon; IL, interleukin; LN, lymph node; PBS, phosphate-buffered saline; $PM_{2.5}$, ambient particulate matter with an aerodynamic diameter of ≤2.5 μm; SEM, standard error of the mean; t-SNE, t-stochastic neighbor embedding; Tfh, T follicular helper; Tfr, T follicular regulatory.

PBS group and the HDM group, their numbers and proportions were not significantly different between the HDM group and the HDM plus $PM_{2.5}$ group (Figure 2E–J). Mice exposed to HDM exhibited a higher proportion and number of Tfh cells compared with those seen in mice exposed to PBS alone. The HDM plus $PM_{2.5}$ group had a significantly higher proportion and number of Tfh cells compared with the PBS group and the HDM group, suggesting preferential regulation of the Tfh subset by $PM_{2.5}$ (Figure 2K,L). It has been reported that cytokine-skewed Tfh cells contribute to class-switch recombination and modify B-cell maturation within GCs.[29] Thus, we examined the proportion and number of IL-4–, IL-17–, and IFN-γ–expressing Tfh cells in each group. As expected, the proportion and number of IL-4–expressing Tfh2 cells was significantly higher in the HDM plus $PM_{2.5}$ group compared with those noted in the PBS group or HDM group (Figure 2M,N).

Next, we used flow cytometry to further confirm Tfh cells and Tfr cells as identified by $CD4^+CXCR5^+ICOS^+Foxp3^-$ cells and $CD4^+CXCR5^+ICOS^+Foxp3^+$ cells, respectively. The Tfh cells and Tfr cells were also determined by PD1 expression. As previously reported, mice in the HDM group showed higher percentages of both Tfh and Tfr cell populations compared with mice in the PBS group.[30] However, mice exposed to HDM plus $PM_{2.5}$ had a significantly higher percentage of Tfh cells compared with those exposed to HDM alone, but those mice exposed to HDM plus $PM_{2.5}$ had only a slightly higher percentage of Tfr cells, which did not reach statistical significance as compared with those exposed to HDM alone (Figure S6A–F).

Measurements of Tfh Differentiation, Allergen-Specific Antibody Production, and Lung Inflammation with Exposure to IP

We next investigated whether IP affects Tfh cell differentiation during the antigen sensitization period. To this end, female C57BL/6 mice were intratracheally sensitized with saline control (PBS), HDM, or HDM plus IP daily from day 0 to day 2. The PBS group was challenged intratracheally with PBS; the HDM group and the HDM plus IP group were challenged intratracheally with HDM from day 9 to day 12 (Figure 3A). As expected, the mice exposed to IP during sensitization had significantly more inflammatory cells in the BALF (Figure 3B,C) and higher serum levels of total IgE, total IgG1, HDM-specific IgE, and HDM-specific IgG1 mAbs (Figure 3D–G). In the mediastinal LNs, the HDM plus IP group had a significantly higher percentage of Tfh cells and $PD1^{hi}$ Tfh cells (Figure 3H,I).

The Effects of AhR Axis on Tfh Cell Differentiation

We hypothesized that the $PM_{2.5}$–AhR axis may affect the differentiation of Tfh cells. To explore this hypothesis, we tested whether AhR in $CD4^+$ T cells is required for the $PM_{2.5}$-mediated increase in the percentage of Tfh cells. Mice with a CD4-specific deletion of AhR ($CD4^{\Delta AhR}$) were generated by crossing AhR^{loxp} mice with CD4-Cre mice. Female $CD4^{\Delta AhR}$ and AhR^{loxp} (as a WT control) mice were intratracheally sensitized with PBS, HDM, and HDM plus $PM_{2.5}$ daily from day 0 to day 2 followed by an intratracheal challenge with PBS or HDM from day 9 to day 12. In the HDM group, there was no significant difference in the Tfh or $PD1^{hi}$ Tfh cell population (Figures 4A, S7A, and S8), Tfr, or $PD1^{hi}$ Tfr cell population (Figures 4B, S7B, and S8), $PD1^{hi}$Tfh/$PD1^{hi}$Tfr ratio (Figures 4C and S7C), and lung inflammation (Figure 4D–F) between AhR^{loxp} mice and $CD4^{\Delta AhR}$ mice. However, in the HDM plus $PM_{2.5}$ group, $CD4^{\Delta AhR}$ mice showed a significantly lower percentage of Tfh cell population (Figure 4A), Tfh/Tfr ratio (Figure 4C), and lung inflammation (Figures 4D–F and S7D,E) compared with control AhR^{loxp} mice.

Next, we performed polarization assays using Tfh cells in the presence of IP *in vitro*. Tfh cells were differentiated from $CD4^+$ naïve T cells under Tfh cell–skewing conditions. IP was added to the cell culture medium for 6 d at a concentration of 30 nM or 300 nM, and the medium and compound were replaced every 3 d. IP treatment significantly promoted Tfh cell differentiation in a dose-dependent manner compared with controls (Figures 5A,B, S9, S10A, S10B, and S11). Consistent with the flow cytometric results, cells exposed to IP exposure also exhibited a higher expression of Tfh-associated genes, including *Bcl-6, Batf, c-Maf*, interferon regulatory factor 4 (*Irf4*), thymocyte selection-associated high mobility group box family member 2 (*Tox2*), and *Il21* (Figure 5C–H), as well as the AhR target gene, *Cyp1a1* (Figure 1). We also found that cells exposed to IP had higher *Il4* expression in Tfh cells, which is required for IgE class switching (Figure 5J). To further characterize the contribution of AhR to IP-induced Tfh cell differentiation, WT Tfh cells and AhR KO Tfh cells were treated with IP or vehicle control, and *Bcl-6*, *Irf4*, and *Il21* expression levels were analyzed by RT-qPCR. Tfh cells had lower levels of *Bcl-6*, *Irf4*, and *Il21* in the AhR KO group (Figure 5K–M). Similarly, Tfh cells exposed to IP and the AhR antagonist, CH-223191, had significantly lower expression of *Bcl-6*, *Irf4*, and *Il21* compared with those exposed to IP alone (Figure 5N–P).

The Effects of IP–AhR–c-Maf Axis on Regulation of Il4 *and* Il21 *Expression in Tfh Cells*

We hypothesized that upon ligand binding, AhR would translocate to the nucleus and interact with cellular musculoaponeurotic fibrosarcoma (c-Maf), allowing the AhR–c-Maf complex to bind to the promoter region of *Il4* and *Il21* to transactivate the expression of *Il4* and *Il21*. To test our hypothesis, c-Maf was knocked down in the Tfh differentiation conditions with or without IP treatment in *vitro*. We found that IP exposure induced higher percentages of $CXCR5^+ICOS^+$ and $CXCR5^+ICOS^+Bcl\text{-}6^+$ Tfh cells in scramble control groups, but this was impaired in the c-Maf knockdown groups (Figure 6A,B). The IP-induced higher expression of Tfh-associated genes, including *Bcl-6, Il21*, and *Il4*, was also lower in c-Maf knockdown cells (Figure 6C–F), but c-Maf knockdown did not appear to affect the expression of the AhR downstream gene, *Cyp1a1* (Figure 6G). We next sought to identify the transcriptional factor binding motifs of AhR and c-Maf at the *Il21* and *Il4* promoters. We found that the *Il21* promoter has two putative AhR-binding sites [xenobiotic response element 1 (XRE1) and XRE2] and three putative c-Maf-binding sites [Maf recognition element 1 (MARE1), MARE2, and MARE3] (Figure 6H). Moreover, three putative XREs (XRE1, XRE2, and XRE3) and two MAREs (MARE1 and MARE2) were predicted in the *Il4* promoter (Figure 6I). To confirm that AhR and c-Maf also interact with their target sequences in the *Il21* promoters under IP treatment, we performed ChIP assays with differentiated Tfh cells *in vitro*. At the *Il21* promoter in Tfh cells, c-Maf interacted with MARE1-3, and AhR interacted with XRE1 and XRE2. With IP treatment, the AhR and c-Maf occupancy at the *Il21* promoter was greater in Tfh cells than in the DMSO control group. No AhR or c-Maf interaction with the XRE or MARE sequences, respectively, at the *Il21* promoter was detected when we used isotype control antibodies (Figure 6J,K). Compared with that seen in Th0 cells, AhR interacted with XRE1 and XRE3 at the *Il4* promoter in Tfh cells, and c-Maf interacted with MARE2 at the *Il4* promoter in Tfh cells; in addition, IP treatment resulted in higher AhR and c-Maf occupancy of the *Il4* promoter in Tfh cells than in the DMSO control group (Figure 6L,M).

To test whether AhR and c-Maf physically interact with each other in Tfh cells, we performed immunoprecipitation followed

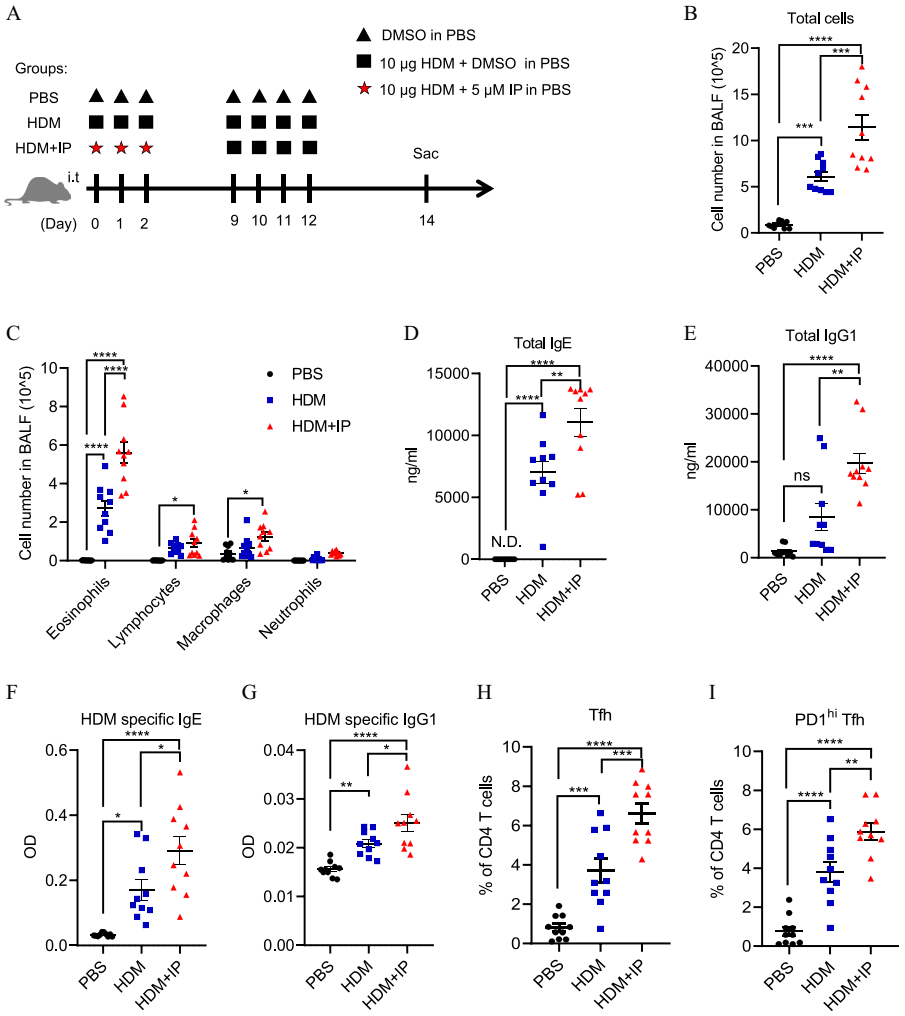

Figure 3. The effects of IP treatment on lung inflammation and Tfh cell differentiation *in vivo*. (A) Mouse allergic lung inflammation model used in the present study (schematic). Mice in the house dust mite (HDM) group were sensitized by intratracheal inhalation of 10 μg of HDM dissolved in 50 μL of PBS per mouse on days 0, 1, and 2 and challenged on days 9, 10, 11, and 12 with the same amount of HDM. Mice in the HDM plus IP group were sensitized by intratracheal inhalation of 10 μg of HDM mixed with IP (5 μM/mouse) in a final volume of 50 μL per mouse on days 0, 1, and 2 and challenged on days 9, 10, 11, and 12 with 10 μg of HDM only. The PBS group mice received 50 μL of PBS during the sensitization and the challenge phases. DMSO was used as the vehicle control in the PBS and the HDM groups to make the comparison with the HDM plus IP group, and the mice were sacrificed and evaluated 48 h after the last allergen challenge. (B) Total cell number in bronchoalveolar lavage fluid (numerical values are shown in Excel Table S44). (C) Cell number of eosinophils, lymphocytes, macrophages, and neutrophils in bronchoalveolar lavage fluid (numerical values are shown in Excel Table S45). The (D) total IgE (numerical values are shown in Excel Table S46), (E) total IgG1 (numerical values are shown in Excel Table S47), (F) HDM-specific IgE (numerical values are shown in Excel Table S48), and (G) HDM-specific IgG1 (numerical values are shown in Excel Table S49) in serum were measured by ELISA. Flow cytometry analysis of the percentage of (H) Tfh (numerical values are shown in Excel Table S50) and (I) $PD1^{hi}$ Tfh (numerical values are shown in Excel Table S51) in $CD4^+$ T cells in lung LNs. All data are representative of two or three independent experiments. $n = 10$ each group. Data are shown as the means ± SEMs. ns, not significant; $^*p < 0.05$, $^{**}p < 0.01$, $^{***}p < 0.001$, and $^{****}p < 0.0001$ according to ANOVA followed by Bonferroni's multiple comparisons test. Note: ANOVA, analysis of variance; BALF, bronchoalveolar lavage fluid; DMSO, dimethyl sulfoxide; ELISA, enzyme-linked immunosorbent assay; Ig, immunoglobulin; IP, indeno [1,2,3-*cd*]pyrene; LN, lymph node; OD, optical density; PBS, phosphate-buffered saline; SEM, standard error of the mean; Tfh, T follicular helper.

by western blotting analysis. Results showed that AhR and c-Maf expression was higher in Tfh cells with IP treatment. Moreover, the c-Maf and AhR complex could be immunoprecipitated in Tfh cells using anti-AhR antibodies and probed with antic-Maf antibodies, suggesting that AhR physically interacted with c-Maf (Figure 6N). In addition, the AhR and c-Maf interaction was enhanced in Tfh cells with IP treatment.

Discussion

Recent studies have implicated the role of Tfh cells in infections and vaccine responses,[31] and dysregulation of Tfh and Tfr cells has been suggested as a critical player in various autoimmune diseases,[31] inflammatory disorders,[32] and cancer.[33] However, the molecular mechanism by which Tfh cells are regulated remains to be fully defined. The results from the present study provide evidence supporting a role of environmental $PM_{2.5}$ and IP in targeting Tfh cell differentiation via AhR, suggesting the potential importance of the $PM_{2.5}$–AhR–c-Maf axis in the regulation of Tfh cell differentiation.

A previous study has shown that AhR and c-Maf interaction triggers the production of IL-21 in IL-27–induced regulatory type 1 cells.[34] c-Maf promotes the differentiation of Tfh cells by increasing IL-21 secretion, and the Tfh function by increasing IL-4 secretion.[35] In the present study, using IP as a model of PAH exposure, it was shown that IP activated AhR to bind with c-Maf, which promoted transactivation of the *Il21* and *Il4* promoters, suggesting that IL-21 production is required for Tfh

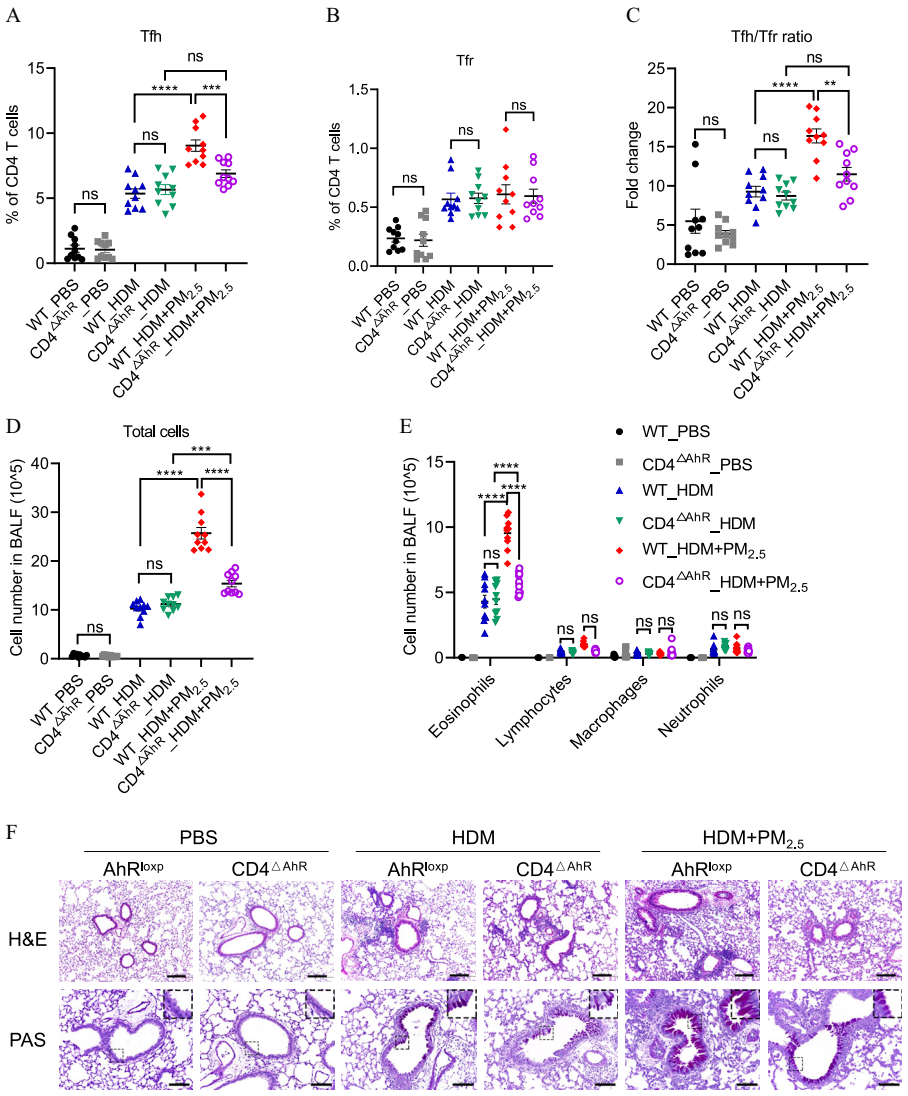

Figure 4. The effects of AhR deficiency in $CD4^+$ T cells on $PM_{2.5}$-induced Tfh cell differentiation. $CD4^{\Delta AhR}$ and AhR^{loxp} (WT) mice were sensitized and challenged, as described in Figure 1A, with or without HDM or $PM_{2.5}$ treatments at the indicated time points, and mice were sacrificed for sampling 48 h after the last allergen challenge. The percentage of (A) Tfh cells (numerical values are shown in Excel Table S52) and (B) Tfr cells (numerical values are shown in Excel Table S54), as well as the (C) Tfh/Tfr ratio (numerical values are shown in Excel Table S56) in $CD4^+$ T cells in lung LNs were examined by flow cytometry analysis. (D) Total cell number in bronchoalveolar lavage fluid (numerical values are shown in Excel Table S58). (E) Cell number of eosinophils, lymphocytes, macrophages, and neutrophils in bronchoalveolar lavage fluid (numerical values are shown in Excel Table S59). (F) Representative H&E and PAS staining of lung tissue sections (scale bar: 500 μm in H&E; scale bar: 200 μm in PAS). The small boxes show the locations of the big boxes in these panels. All data are representative of two or three independent experiments. $n = 10$ each group. Data are shown as the means ± SEMs. ns, not significant; $^*p < 0.05$, $^{**}p < 0.01$, $^{***}p < 0.001$, and $^{****}p < 0.0001$ according to ANOVA followed by Bonferroni's multiple comparisons test. Note: AhR, aryl hydrocarbon receptor; ANOVA, analysis of variance; BALF, bronchoalveolar lavage fluid; H&E, hematoxylin and eosin; HDM, house dust mite; LN, lymph node; PAS, periodic acid–Schiff; PBS, phosphate-buffered saline; $PM_{2.5}$, ambient particulate matter with an aerodynamic diameter of ≤2.5 μm; SEM, standard error of the mean; Tfh, T follicular helper; Tfr, T follicular regulatory; WT, wild type.

cell differentiation and IL-4 production in Tfh cells to promote IgE class-switch recombination in B cells. Although a previous study showed the links between $PM_{2.5}$ exposure, allergic sensitization, asthma, and Th17 activation,[36] our data provide another potentially important regulatory mechanism involving the $PM_{2.5}$–AhR axis in Tfh cells. Collectively, these results add a potentially new dimension in the understanding of Tfh cell differentiation and function, which, together with those potential targets of $PM_{2.5}$ exposure, including B cells,[37] Th2,[38] and Th17,[36,39] aggravate allergen-induced pulmonary allergic responses.

Tfh cell differentiation is a multistep process, in which DCs are necessary and sufficient to induce the Tfh cell intermediate that requires additional interactions with distinct APCs for promoting the full differentiation program of Tfh cells.[40,41] Our data showed that the frequency of the migratory DC-1 subset with high expression of programmed cell death 1 ligand 1 (PDL1) and PDL2 was greater after HDM treatment *in vivo*. However, there was no difference in the proportion of resident DCs and migratory DCs between the HDM and HDM plus $PM_{2.5}$ groups, suggesting that $PM_{2.5}$ exposure did not alter the proportion of resident DCs and migratory DCs in LNs. In addition to DCs, a small population of cells, which were defined as macrophages, was significantly higher in the HDM plus $PM_{2.5}$ group compared with the PBS and HDM groups. Interestingly, the specific subset of the macrophage population expressed IL-4 and IFN-γ, which may play a role in the overall mechanism of regulation by $PM_{2.5}$ exposure.

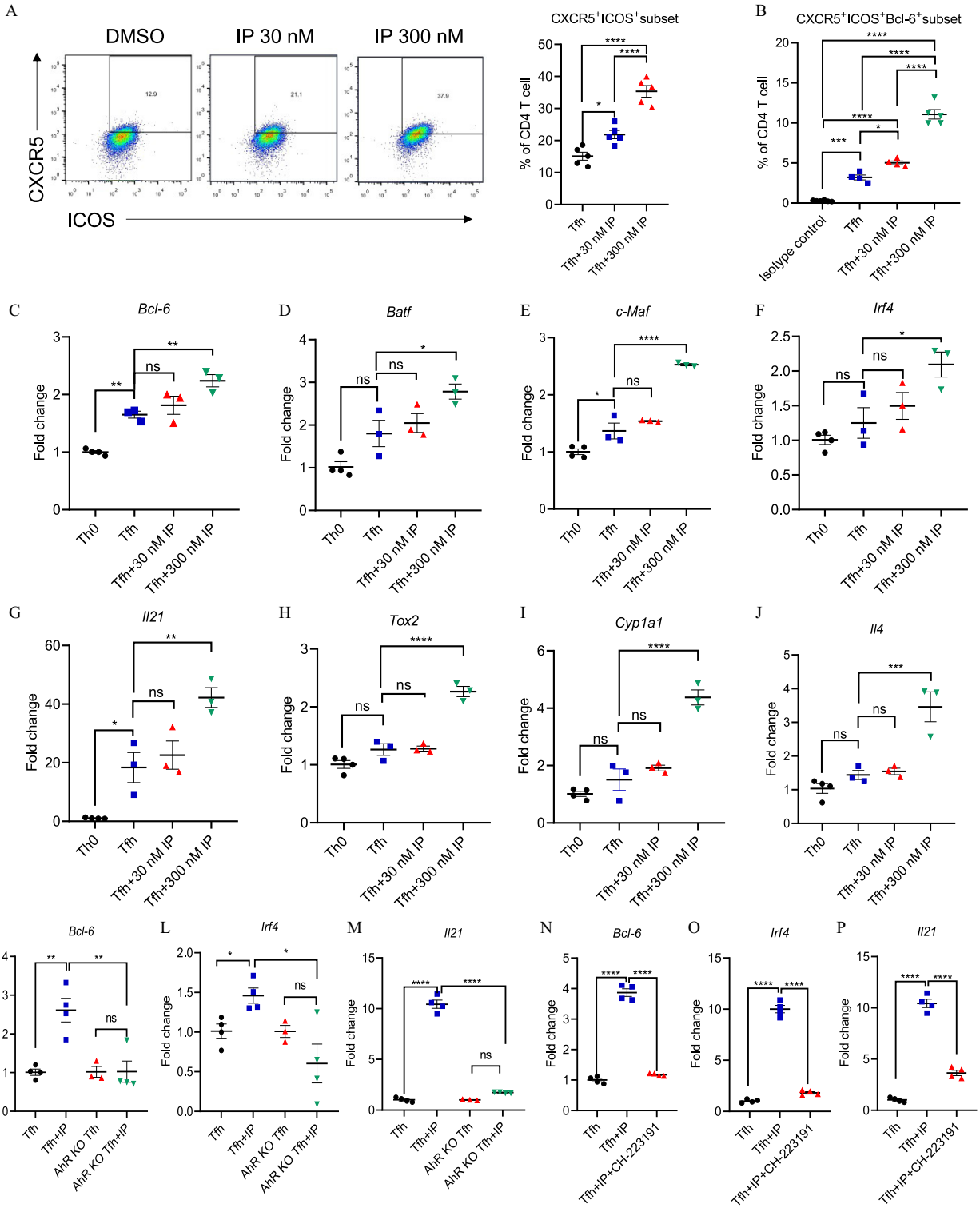

Figure 5. The effects of IP treatment on Tfh cell differentiation *in vitro*. IP was added to cell culture medium for 6 d at a concentration of 30 nM or 300 nM, the medium and compound were replaced every 3 d during Tfh cell differentiation. Flow cytometry analysis of the percentages of the (A) $CD4^+ICOS^+CXCR5^+$ (numerical values are shown in Excel Table S62) and (B) $CD4^+ICOS^+CXCR5^+Bcl\text{-}6^+$ (numerical values are shown in Excel Table S63) subsets in $CD4^+$ T cells. (C–J) Tfh-associated genes were evaluated by RT-qPCR (numerical values are shown in Excel Tables S66–S73). (K–M) WT and AhR KO Tfh cells were treated with IP at a concentration of 30 nM or 300 nM, and the mRNA expression levels of *Bcl-6, Irf4,* and *Il21* were examined by RT-qPCR (numerical values are shown in Excel Tables S74–S76). (N–P) The mRNA expression levels of *Bcl-6, Irf4,* and *Il21* were examined in Tfh cells treated with IP or IP plus AhR inhibitor (CH-223191; 10 μM) (numerical values are shown in Excel Tables S77–S79). DMSO was the vehicle for IP and CH-223191, and all experiments were done in the presence of the DMSO (0.01%) as vehicle control. All data are representative of two or three independent experiments. $n = 3$–5 each group. Data are shown as the means ± SEMs. ns, not significant; $^*p < 0.05$, $^{**}p < 0.01$, $^{***}p < 0.001$, and $^{****}p < 0.0001$ according to ANOVA followed by Bonferroni's multiple comparisons test. Note: AhR, aryl hydrocarbon receptor; ANOVA, analysis of variance; DMSO, dimethyl sulfoxide; IP, indeno[1,2,3-*cd*]pyrene; KO, knockout; RT-qPCR, quantitative reverse transcription polymerase chain reaction; SEM, standard error of the mean; Tfh, T follicular helper; WT, wild type.

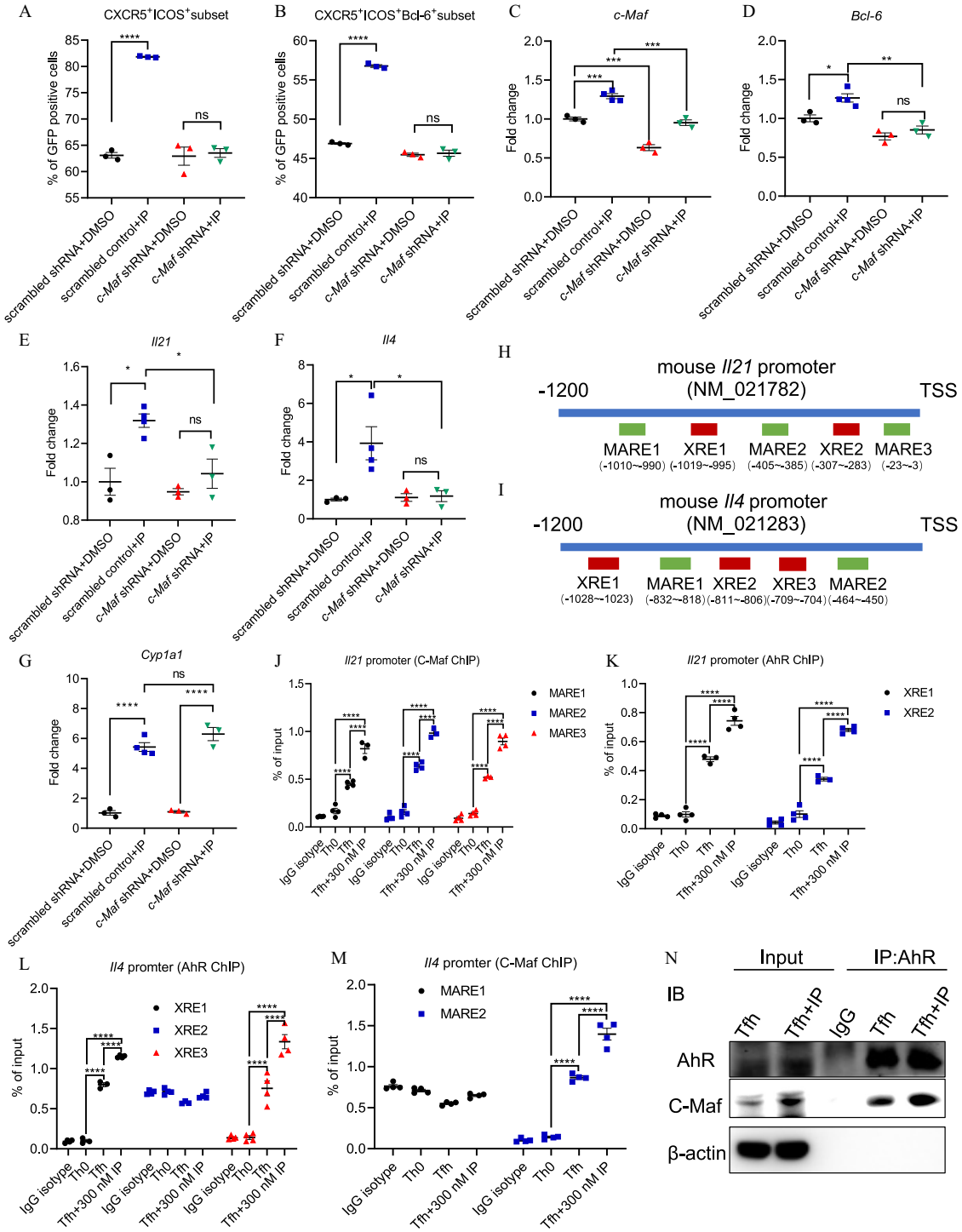

Figure 6. The effects of AhR and c-Maf on IP-induced Tfh cell differentiation *in vitro*. Flow cytometry analysis of the (A) $CD4^+CXCR5^+ICOS^+$ subset and (B) $CD4^+CXCR5^+ICOS^+Bcl\text{-}6^+$ subset in GFP^+ cells (*c-Maf* shRNA-expressing cells) (numerical values are shown in Excel Tables S80 and S81). (C–G) The mRNA expression levels of *c-Maf*, *Bcl-6*, *Il21*, *Il4* and *Cyp1a1* in *c-Maf*-knockdown cells were measured by RT-qPCR (numerical values are shown in Excel Tables S82–S86). (H) Schematic diagram of AhR- and c-Maf-binding sites (XRE and MARE) in the *Il21* promotor region. (I) Schematic diagram of the AhR- and c-Maf-binding sites (XRE and MARE) in the *Il4* promotor region. IP was added to the cell culture medium at a concentration of 30 nM or 300 nM during Tfh cell differentiation. Immunoprecipitation test of c-Maf- and AhR- binding levels in Tfh cells. Chromatin immunoprecipitation (ChIP) assay of the and (J) c-Maf- and (K) AhR-binding levels at the *Il21* promotor region in Th0 cells, Tfh cells, IP-treated Tfh cells, and IgG isotype control (numerical values are shown in Excel Tables S87 and S88). ChIP assay of the (L) AhR- and (M) c-Maf-binding levels at the *Il4* promotor region in Th0 cells, Tfh cells, IP-treated Tfh cells, and IgG isotype control (numerical values are shown in Excel Tables S89 and S90). (N) The AhR and c-Maf interaction in Tfh cells and IP-treated Tfh cells was examined by immunoprecipitation assay and western blotting. DMSO was the vehicle for IP and all experiments were done in the presence of the DMSO (0.01%) as vehicle control. All data are representative of two or three independent experiments. $n = 3$–4 each group. Data are shown as the means ± SEMs. ns, not significant; $^*p < 0.05$, $^{**}p < 0.01$, $^{***}p < 0.001$, and $^{****}p < 0.0001$ according to ANOVA followed by Bonferroni's multiple comparisons test. Note: AhR, aryl hydrocarbon receptor; ANOVA, analysis of variance; ChIP, chromatin immunoprecipitation; c-Maf, cellular musculoaponeurotic fibrosarcoma; DMSO, dimethyl sulfoxide; GFP, green fluorescent protein; Ig, immunoglobulin; IL, interleukin; IP, indeno[1,2,3-*cd*]pyrene; MARE, Maf recognition element; RT-qPCR, quantitative reverse transcription polymerase chain reaction; SEM, standard error of the mean; shRNA, short hairpin RNA; Tfh, T follicular helper; Th0, immature T helper cell; TSS, transcription start site; XRE, xenobiotic response element.

In contrast to our study, in a mouse model of acute influenza infection, administration of AhR ligands, 2,3,7,8-tetrachlorodibenzo-*p*-dioxin (TCDD), 3,3′,4,4′,5 pentachlorobiphenyl (PCB 126) and an endogenous agonist, 2-(1*H*-indol-3-ylcarbonyl)-4-thiazolecarboxylic acid methyl ester (ITE) reduced the Tfh cells, whereas administration of another endogenous agonist, 6-formylindolo[3,2-b]carbazole (FICZ) increased their frequency.[42] The follow-up study suggested that oral delivery of TCDD reduced Tfh cell differentiation and T-cell–dependent B-cell responses in mice after acute influenza infection,[43] although its suppressive mechanism was unclear. These contrasting results suggest that different AhR ligands and their dosage and the route of administration may exert differential outcomes. Similar ligand- and dose-dependent outcomes have been noted in the case of Treg and DC regulation by TCDD vs. $PM_{2.5}$/IP.[24,44–46] Another study reported that TCDD exposure in a rat model before HDM sensitization was shown to suppress the immune response to HDM.[47] We also reported that TCDD suppressed, whereas IP increased, total IgE and antigen-specific IgE levels in a mouse allergic lung inflammation model.[46,48] Indeed, although the functional impact of the AhR–ligand axis in various pathophysiological contexts has been well documented, the molecular basis and features governing the AhR signaling and its transcriptional activity remain to be fully elucidated. It is now recognized that its functional outcomes are ligand,[42] cell type,[49,50] and context[44,45] dependent, wherein the ligand's structural feature,[51] the dosage used, and the timing of exposure[52] are known to influence the activation of AhR and its subsequent nuclear translocation and binding of transcriptional co-activators; also, the ligand's half-life *in vivo* may also determine the final outcome. Therefore, differential AhR signaling upon interaction with different ligands can be logically anticipated, particularly in the context of different model systems, such as allergic inflammation vs. respiratory infection, with a distinct molecular and cellular network of regulation.

Because it is challenging to examine human Tfh cells in secondary lymphoid organs, such as tonsils, spleen, and LNs, the alternative approach is to examine circulating $CXCR5^+CD4^+$ Tfh (cTfh) cells in human peripheral blood samples. The frequency of cTfh cells is positively correlated with serum IgE levels, and cTfh cells from patients with asthma more effectively promote IgE production than cTfh cells from healthy control study participants.[53] Furthermore, the skewing of cTfh cells toward cTfh2 cells has been observed in patients with asthma, and the positive correlation of serum PAH and IL-4 levels has been noted in children with asthma.[54] In addition, the patients with asthma treated with inhaled corticosteroids show significantly lower frequencies of cTfh2 and $ICOS^+$ cTfh cells, as well as improved asthma symptoms.[55] Our mouse model and single-cell mass cytometry analysis provide a comprehensive analysis and plausible mechanism linking $PM_{2.5}$ exposure, IgE production, and allergic disease, in which the AhR–c-Maf axis–mediated Tfh cell differentiation is a prominent mechanistic feature.

Acknowledgments

K.L., Y.G., W.X., J.F., and S.H. designed and carried out experiments and analyzed the data. S.H., X.X., and X.H. contributed critical reagents and protocols. K.L., S.H., and Y.Z. wrote the manuscript. S.H. and Y.Z. planned, designed, supervised, and coordinated the overall research efforts.

This work was supported by grants from the National Key R&D Program of China (2021YFC2701800 and 2021YFC2701802 to Y.Z.), National Natural Science Foundation of China (82241038 and 81974248 to Y.Z.; 82100033 to S.H.), Program for Outstanding Medical Academic Leader (2019LJ19 to Y.Z.), Shanghai Committee of Science and Technology (21140902400 to Y.Z.; 23ZR1407600, 21ZR1410000 and 19ZR1406400 to JF; 20ZR1408300 to X.H.), the International Joint Laboratory Program of National Children's Medical Center (EK1125180109 to Y.Z.), Shanghai Municipal Planning Commission of Science and Research Fund (20214Y0440 to S.H.), Shenzhen Third Affiliated Hospital of Shenzhen University Postdoctoral Fellowship, Shenzhen Science and Technology Peacock Team Project (KQTD20170331145453160 to S.H.), and National Health Research Institutes, Taiwan (EM-109-PP-10 to S.H.).

References

1. Fahy JV. 2015. Type 2 inflammation in asthma—present in most, absent in many. Nat Rev Immunol 15(1):57–65, PMID: 25534623, https://doi.org/10.1038/nri3786.
2. Gowthaman U, Chen JS, Zhang B, Flynn WF, Lu Y, Song W, et al. 2019. Identification of a T follicular helper cell subset that drives anaphylactic IgE. Science 365(6456):eaaw6433, PMID: 31371561, https://doi.org/10.1126/science.aaw6433.
3. Kobayashi T, Iijima K, Dent AL, Kita H. 2017. Follicular helper T cells mediate IgE antibody response to airborne allergens. J Allergy Clin Immunol 139(1):300–313.e7, PMID: 27325434, https://doi.org/10.1016/j.jaci.2016.04.021.
4. Xue M, Xu S, Su L, He S, Wu B, Ji C, et al. 2021. Surfactant protein-A inhibits thymic stromal lymphopoietin-mediated T follicular helper cell differentiation and IgE production in asthma. Clin Immunol 231:108822, PMID: 34400320, https://doi.org/10.1016/j.clim.2021.108822.
5. Gowthaman U, Chen JS, Eisenbarth SC. 2020. Regulation of IgE by T follicular helper cells. J Leukoc Biol 107(3):409–418, PMID: 31965637, https://doi.org/10.1002/JLB.3RI1219-425R.
6. Ise W, Fujii K, Shiroguchi K, Ito A, Kometani K, Takeda K, et al. 2018. T follicular helper cell-germinal center B cell interaction strength regulates entry into plasma cell or recycling germinal center cell fate. Immunity 48(4):702–715.e4, PMID: 29669250, https://doi.org/10.1016/j.immuni.2018.03.027.
7. Qi H, Chen X, Chu C, Liu D, Ma W, Wang Y, et al. 2014. Tfh cell differentiation and their function in promoting B-cell responses. Adv Exp Med Biol 841:153–180, PMID: 25261207, https://doi.org/10.1007/978-94-017-9487-9_6.
8. Olatunde AC, Hale JS, Lamb TJ. 2021. Cytokine-skewed Tfh cells: functional consequences for B cell help. Trends Immunol 42(6):536–550, PMID: 33972167, https://doi.org/10.1016/j.it.2021.04.006.
9. Nurieva RI, Chung Y, Martinez GJ, Yang XO, Tanaka S, Matskevitch TD, et al. 2009. Bcl6 mediates the development of T follicular helper cells. Science 325(5943):1001–1005, PMID: 19628815, https://doi.org/10.1126/science.1176676.
10. Yu D, Rao S, Tsai LM, Lee SK, He Y, Sutcliffe EL, et al. 2009. The transcriptional repressor Bcl-6 directs T follicular helper cell lineage commitment. Immunity 31(3):457–468, PMID: 19631565, https://doi.org/10.1016/j.immuni.2009.07.002.
11. Johnston RJ, Poholek AC, DiToro D, Yusuf I, Eto D, Barnett B, et al. 2009. Bcl6 and Blimp-1 are reciprocal and antagonistic regulators of T follicular helper cell differentiation. Science 325(5943):1006–1010, PMID: 19608860, https://doi.org/10.1126/science.1175870.
12. Nurieva RI, Chung Y, Hwang D, Yang XO, Kang HS, Ma L, et al. 2008. Generation of T follicular helper cells is mediated by interleukin-21 but independent of T helper 1, 2, or 17 cell lineages. Immunity 29(1):138–149, PMID: 18599325, https://doi.org/10.1016/j.immuni.2008.05.009.
13. Read KA, Powell MD, Oestreich KJ. 2016. T follicular helper cell programming by cytokine-mediated events. Immunology 149(3):253–261, PMID: 27442976, https://doi.org/10.1111/imm.12648.
14. Morita R, Schmitt N, Bentebibel SE, Ranganathan R, Bourdery L, Zurawski G, et al. 2011. Human blood $CXCR5^+CD4^+$ T cells are counterparts of T follicular cells and contain specific subsets that differentially support antibody secretion. Immunity 34(1):108–121, PMID: 21215658, https://doi.org/10.1016/j.immuni.2010.12.012.
15. Akiyama M, Yasuoka H, Yoshimoto K, Takeuchi T. 2018. Interleukin-4 contributes to the shift of balance of IgG subclasses toward IgG4 in IgG4-related disease. Cytokine 110:416–419, PMID: 29861381, https://doi.org/10.1016/j.cyto.2018.05.009.
16. Sahoo A, Alekseev A, Tanaka K, Obertas L, Lerman B, Haymaker C, et al. 2015. Batf is important for IL-4 expression in T follicular helper cells. Nat Commun 6(1):7997, PMID: 26278622, https://doi.org/10.1038/ncomms8997.
17. Cheng Q, Yang CY, Guo BY, Wei X, Liu M. 2017. Analysis of mechanism of PM2.5 and house dust mite antigen Der p1 in attack stage of child asthma. Eur Rev Med Pharmacol Sci 21(10):2458–2462, PMID: 28617540.
18. Rosenquist NA, Metcalf WJ, Ryu SY, Rutledge A, Coppes MJ, Grzymski JJ, et al. 2020. Acute associations between $PM_{2.5}$ and ozone concentrations and asthma exacerbations among patients with and without allergic comorbidities. J Expo Sci Environ Epidemiol 30(5):795–804, PMID: 32094459, https://doi.org/10.1038/s41370-020-0213-7.

19. Zhao C, Wang Y, Su Z, Pu W, Niu M, Song S, et al. 2020. Respiratory exposure to PM2.5 soluble extract disrupts mucosal barrier function and promotes the development of experimental asthma. Sci Total Environ 730:139145, PMID: 32402975, https://doi.org/10.1016/j.scitotenv.2020.139145.
20. Chang KF, Fang GC, Chen JC, Wu YS. 2006. Atmospheric polycyclic aromatic hydrocarbons (PAHs) in Asia: a review from 1999 to 2004. Environ Pollut 142(3):388–396, PMID: 16343719, https://doi.org/10.1016/j.envpol.2005.09.025.
21. Yu SY, Liu W, Xu YS, Yi K, Zhou M, Tao S, et al. 2019. Characteristics and oxidative potential of atmospheric $PM_{2.5}$ in Beijing: source apportionment and seasonal variation. Sci Total Environ 650(pt 1):277–287, PMID: 30199673, https://doi.org/10.1016/j.scitotenv.2018.09.021.
22. Plé C, Fan Y, Ait Yahia S, Vorng H, Everaere L, Chenivesse C, et al. 2015. Polycyclic aromatic hydrocarbons reciprocally regulate IL-22 and IL-17 cytokines in peripheral blood mononuclear cells from both healthy and asthmatic subjects. PLoS One 10(4):e0122372, PMID: 25860963, https://doi.org/10.1371/journal.pone.0122372.
23. Tajima H, Tajiki-Nishino R, Watanabe Y, Fukuyama T. 2019. Direct activation of aryl hydrocarbon receptor by benzo[a]pyrene elicits T-helper 2-driven proinflammatory responses in a mouse model of allergic dermatitis. J Appl Toxicol 39(7):936–944, PMID: 30748024, https://doi.org/10.1002/jat.3782.
24. Sun L, Fu J, Lin SH, Sun JL, Xia L, Lin CH, et al. 2020. Particulate matter of 2.5 μm or less in diameter disturbs the balance of T_H17/regulatory T cells by targeting glutamate oxaloacetate transaminase 1 and hypoxia-inducible factor 1α in an asthma model. J Allergy Clin Immunol 145(1):402–414, PMID: 31647966, https://doi.org/10.1016/j.jaci.2019.10.008.
25. Świst K, Pajtasz-Piasecka E. 2011. The influence of transcription factors on $CD4^+$ T cell differentiation [in Polish]. Postepy Hig Med Dosw (Online) 65:414–426, PMID: 21734326, https://doi.org/10.5604/17322693.949499.
26. Qian G, Jiang W, Zou B, Feng J, Cheng X, Gu J, et al. 2018. LPS inactivation by a host lipase allows lung epithelial cell sensitization for allergic asthma. J Exp Med 215(9):2397–2412, PMID: 30021797, https://doi.org/10.1084/jem.20172225.
27. Xu W, Zhao X, Wang X, Feng H, Gou M, Jin W, et al. 2019. The transcription factor Tox2 drives T follicular helper cell development via regulating chromatin accessibility. Immunity 51(5):826–839.e5, PMID: 31732165, https://doi.org/10.1016/j.immuni.2019.10.006.
28. Zhou Y, Do DC, Ishmael FT, Squadrito ML, Tang HM, Tang HL, et al. 2018. Mannose receptor modulates macrophage polarization and allergic inflammation through miR-511-3p. J Allergy Clin Immunol 141(1):350–364.e8, PMID: 28629744, https://doi.org/10.1016/j.jaci.2017.04.049.
29. Mintz MA, Cyster JG. 2020. T follicular helper cells in germinal center B cell selection and lymphomagenesis. Immunol Rev 296(1):48–61, PMID: 32412663, https://doi.org/10.1111/imr.12860.
30. Clement RL, Daccache J, Mohammed MT, Diallo A, Blazar BR, Kuchroo VK, et al. 2019. Follicular regulatory T cells control humoral and allergic immunity by restraining early B cell responses. Nat Immunol 20(10):1360–1371, PMID: 31477921, https://doi.org/10.1038/s41590-019-0472-4.
31. Crotty S. 2019. T follicular helper cell biology: a decade of discovery and diseases. Immunity 50(5):1132–1148, PMID: 31117010, https://doi.org/10.1016/j.immuni.2019.04.011.
32. Uwadiae FI, Pyle CJ, Walker SA, Lloyd CM, Harker JA. 2019. Targeting the ICOS/ICOS-L pathway in a mouse model of established allergic asthma disrupts T follicular helper cell responses and ameliorates disease. Allergy 74(4):650–662, PMID: 30220084, https://doi.org/10.1111/all.13602.
33. Cui C, Wang J, Fagerberg E, Chen PM, Connolly KA, Damo M, et al. 2021. Neoantigen-driven B cell and CD4 T follicular helper cell collaboration promotes anti-tumor CD8 T cell responses. Cell 184(25):6101–6118.e13, PMID: 34852236, https://doi.org/10.1016/j.cell.2021.11.007.
34. Apetoh L, Quintana FJ, Pot C, Joller N, Xiao S, Kumar D, et al. 2010. The aryl hydrocarbon receptor interacts with c-Maf to promote the differentiation of type 1 regulatory T cells induced by IL-27. Nat Immunol 11(9):854–861, PMID: 20676095, https://doi.org/10.1038/ni.1912.
35. Ahearne MJ, Willimott S, Piñon L, Kennedy DB, Miall F, Dyer MJS, et al. 2013. Enhancement of CD154/IL4 proliferation by the T follicular helper (Tfh) cytokine, IL21 and increased numbers of circulating cells resembling Tfh cells in chronic lymphocytic leukaemia. Br J Haematol 162(3):360–370, PMID: 23710828, https://doi.org/10.1111/bjh.12401.
36. Zhang J, Fulgar CC, Mar T, Young DE, Zhang Q, Bein KJ, et al. 2018. T_H17-induced neutrophils enhance the pulmonary allergic response following BALB/c exposure to house dust mite allergen and fine particulate matter from California and China. Toxicol Sci 164(2):627–643, PMID: 29846732, https://doi.org/10.1093/toxsci/kfy127.
37. Villa M, Gialitakis M, Tolaini M, Ahlfors H, Henderson CJ, Wolf CR, et al. 2017. Aryl hydrocarbon receptor is required for optimal B-cell proliferation. EMBO J 36(1):116–128, PMID: 27875245, https://doi.org/10.15252/embj.201695027.
38. Yan LI, Gong C, Ying L, Fu W, Liu S, Dai J, et al. 2019. $PM_{2.5}$ affects establishment of immune tolerance in newborn mice by reducing PD-L1 expression. J Biosci 44(2):41, PMID: 31180054, https://doi.org/10.1007/s12038-019-9858-6.
39. Castañeda AR, Vogel CFA, Bein KJ, Hughes HK, Smiley-Jewell S, Pinkerton KE. 2018. Ambient particulate matter enhances the pulmonary allergic immune response to house dust mite in a BALB/c mouse model by augmenting Th2- and Th17-immune responses. Physiol Rep 6(18):e13827, PMID: 30230272, https://doi.org/10.14814/phy2.13827.
40. Goenka R, Barnett LG, Silver JS, O'Neill PJ, Hunter CA, Cancro MP, et al. 2011. Cutting edge: dendritic cell-restricted antigen presentation initiates the follicular helper T cell program but cannot complete ultimate effector differentiation. J Immunol 187(3):1091–1095, PMID: 21715693, https://doi.org/10.4049/jimmunol.1100853.
41. Deenick EK, Chan A, Ma CS, Gatto D, Schwartzberg PL, Brink R, et al. 2010. Follicular helper T cell differentiation requires continuous antigen presentation that is independent of unique B cell signaling. Immunity 33(2):241–253, PMID: 20691615, https://doi.org/10.1016/j.immuni.2010.07.015.
42. Boule LA, Burke CG, Jin GB, Lawrence BP. 2018. Aryl hydrocarbon receptor signaling modulates antiviral immune responses: ligand metabolism rather than chemical source is the stronger predictor of outcome. Sci Rep 8(1):1826, PMID: 29379138, https://doi.org/10.1038/s41598-018-20197-4.
43. Houser CL, Lawrence BP. 2022. The aryl hydrocarbon receptor modulates T follicular helper cell responses to influenza virus infection in mice. J Immunol 208(10):2319–2330, PMID: 35444027, https://doi.org/10.4049/jimmunol.2100936.
44. Quintana FJ, Basso AS, Iglesias AH, Korn T, Farez MF, Bettelli E, et al. 2008. Control of T_{reg} and T_H17 cell differentiation by the aryl hydrocarbon receptor. Nature 453(7191):65–71, PMID: 18362915, https://doi.org/10.1038/nature06880.
45. Schulz VJ, van Roest M, Bol-Schoenmakers M, van Duursen MBM, van den Berg M, Pieters RHH, et al. 2013. Aryl hydrocarbon receptor activation affects the dendritic cell phenotype and function during allergic sensitization. Immunobiology 218(8):1055–1062, PMID: 23433705, https://doi.org/10.1016/j.imbio.2013.01.004.
46. Wong TH, Lee CL, Su HH, Lee CL, Wu CC, Wang CC, et al. 2018. A prominent air pollutant, indeno[1,2,3-cd]pyrene, enhances allergic lung inflammation via aryl hydrocarbon receptor. Sci Rep 8(1):5198, PMID: 29581487, https://doi.org/10.1038/s41598-018-23542-9.
47. Luebke RW, Copeland CB, Daniels M, Lambert AL, Gilmour MI. 2001. Suppression of allergic immune responses to house dust mite (HDM) in rats exposed to 2,3,7,8-TCDD. Toxicol Sci 62(1):71–79, PMID: 11399795, https://doi.org/10.1093/toxsci/62.1.71.
48. Xu T, Zhou Y, Qiu L, Do DC, Zhao Y, Cui Z, et al. 2015. Aryl hydrocarbon receptor protects lungs from cockroach allergen-induced inflammation by modulating mesenchymal stem cells. J Immunol 195(12):5539–5550, PMID: 26561548, https://doi.org/10.4049/jimmunol.1501198.
49. Hung CH, Yang SN, Wang YF, Liao WT, Kuo PL, Tsai EM, et al. 2013. Environmental alkylphenols modulate cytokine expression in plasmacytoid dendritic cells. PLoS One 8(9):e73534, PMID: 24039973, https://doi.org/10.1371/journal.pone.0073534.
50. Su HH, Lin HT, Suen JL, Sheu CC, Yokoyama KK, Huang SK, et al. 2016. Aryl hydrocarbon receptor–ligand axis mediates pulmonary fibroblast migration and differentiation through increased arachidonic acid metabolism. Toxicology 370:116–126, PMID: 27697457, https://doi.org/10.1016/j.tox.2016.09.019.
51. Itkin B, Breen A, Turyanska L, Sandes EO, Bradshaw TD, Loaiza-Perez AI. 2020. New treatments in renal cancer: the AhR ligands. Int J Mol Sci 21(10):3551, PMID: 32443455, https://doi.org/10.3390/ijms21103551.
52. Rannug A, Rannug U. 2018. The tryptophan derivative 6-formylindolo[3,2-*b*]carbazole, FICZ, a dynamic mediator of endogenous aryl hydrocarbon receptor signaling, balances cell growth and differentiation. Crit Rev Toxicol 48(7):555–574, PMID: 30226107, https://doi.org/10.1080/10408444.2018.1493086.
53. Gong F, Su Q, Jiang D, Chen J, Pan Y, Huang X. 2014. High frequency of circulating follicular helper T cells in patients with bronchial asthma. Clin Lab 60(6):963–968, PMID: 25016701, https://doi.org/10.7754/Clin.Lab.2013.130427.
54. Al-Daghri NM, Abd-Alrahman S, Draz H, Alkharfy K, Mohammed AK, Clerici MS, et al. 2014. Increased IL-4 mRNA expression and poly-aromatic hydrocarbon concentrations from children with asthma. BMC Pediatr 14(1):17, PMID: 24450480, https://doi.org/10.1186/1471-2431-14-17.
55. Miyajima S, Shigehara K, Kamekura R, Takaki H, Yabe H, Ikegami I, et al. 2020. Activated circulating T follicular helper cells and skewing of T follicular helper 2 cells are down-regulated by treatment including an inhaled corticosteroid in patients with allergic asthma. Allergol Int 69(1):66–77, PMID: 31648923, https://doi.org/10.1016/j.alit.2019.08.008.